Forschungszentrum Karlsruhe
Technik und Umwelt

Wissenschaftliche Berichte
FZKA 6684

Integral activation experiments on fusion relevant materials using a white fast-neutron field

U. von Möllendorff, H. Tsige-Tamirat, H. Giese, F. Maekawa*

Institut für Reaktorsicherheit
Institut für Hochleistungsimpuls- und Mikrowellentechnik
Programm Kernfusion

*Japan Atomic Energy Research Institute

Forschungszentrum Karlsruhe GmbH, Karlsruhe
2002

Impressum der Print-Ausgabe:

Als Manuskript gedruckt
Für diesen Bericht behalten wir uns alle Rechte vor

Forschungszentrum Karlsruhe GmbH
Postfach 3640, 76021 Karlsruhe

Mitglied der Hermann von Helmholtz-Gemeinschaft
Deutscher Forschungszentren (HGF)

ISSN 0947-8620

Abstract

For validating radioactive inventories calculated by the European Activation System (EASY), a series of integral activation experiments in a white fast neutron field ranging up to 20 MeV was conducted within a task of the European Fusion Technology Programme. The irradiated samples were investigated by gamma ray spectrometry. Specific activities in becquerels per kilogram of sample material were derived for many product nuclides, including, in some cases, products of sequential charged particle induced reactions and of exotic neutron reactions such as (n,2p) and (n,pα). Experiments on vanadium alloys, nickel, copper, lithium orthosilicate, Eurofer-97 steel and tungsten are described. The experimental results are given together with sufficient details of each irradiation to allow comparisons with future EASY or other calculations. Also, calculation-over-experiment ratios for EASY-99 calculations and, in cases of single-pathway products, experimental one-group production cross sections are given. Some results given earlier are presented in revised form. For a few product nuclides, results are new and were not presented in our earlier unpublished reports.

Integrale Aktivierungsexperimente an fusionsrelevanten Materialien in einem weißen Feld schneller Neutronen

Zusammenfassung

Zur Überprüfung von Berechnungen radioaktiver Inventare mit dem European Activation System (EASY) wurde im Rahmen einer Aufgabe des Europäischen Fusionstechnologieprogramms eine Serie von integralen Aktivierungsexperimenten in einem weißen Feld schneller Neutronen durchgeführt. Die bestrahlten Proben wurden mittels Gammaspektrometrie untersucht. Spezifische Aktivitäten in Becquerel pro Kilogramm Probenmaterial wurden für viele Produktnuklide bestimmt, darunter in einigen Fällen Produkte aus Reaktionen sekundärer geladener Teilchen und aus exotischen Neutronenreaktionen wie (n,2p) und (n,pα). Es werden Experimente an Vanadiumlegierungen, Nickel, Kupfer, Lithiumorthosilikat, Eurofer-97-Stahl und Wolfram beschrieben. Die Meßergebnisse werden zusammen mit genügend Details der Bestrahlungen angegeben, um Vergleiche mit zukünftigen EASY- oder anderen Berechnungen zu ermöglichen. Auch Rechnung-Experiment-Verhältnisse für EASY-99-Rechnungen sowie bei Produkten aus einem eindeutigen Erzeugungspfad die experimentellen 1-Gruppen-Wirkungsquerschnitte werden angegeben. Einige früher angegebene Ergebnisse werden in revidierter Form vorgelegt. Für einige Nuklide werden neue, in den bisherigen unveröffentlichten Berichten nicht enthaltene Ergebnisse angegeben.

Contents **Page**

1 INTRODUCTION

Radioactivity induced in structural and other materials is an important problem in any nuclear technology that involves free neutrons. Because of the high energy of fusion neutrons, activation in fusion neutron fields is generally different from and more complex than activation in fission neutron fields. In many of the possible nuclear reactions induced by fast neutrons, charged particles are emitted. This constitutes transmutation, i.e., the resulting product nuclide has a lower atomic number than the target nuclide and is thus a different chemical element. The typical kinetic energy of a neutron produced in the D+T fusion reaction, 14 MeV, is higher than the binding energy of a neutron or proton in any nucleus. Consequently, not only the reaction types (n,n'), (n,p) and (n,α) are possible, but also those in which two free particles or a loosely bound light nucleus are emitted, such as (n,2n), (n,nα), (n,d), (n,t), (n,^{3}He) and others. Each of these reaction types leads from the same given target nuclide to a different product nuclide. Irradiation of a pure target nuclide may thus result in several different radionuclides being produced simultaneously. Inversely, in irradiation of a multi-isotope element or a combination of elements of neighbouring atomic numbers, such as, e.g., a chromium-nickel steel, a given radionuclide may be produced simultaneously by different reactions on different target nuclides.

As fusion neutron fields contain relatively few epithermal and thermal neutrons, the (n,γ) reactions ('neutron capture') are, generally, not dominating to the same extent as they are in the activation in fission reactors. Rather, the predominant reaction types are (n,p), (n,α) and (n,2n).

The fast charged particles emitted from reactions can induce further reactions on nuclei present in the irradiated material (Sequential Charged Particle Reactions, SCPR). In this way, a target of atomic number Z can be transmuted into a product nuclide with atomic number Z+1 or even Z+2, which is impossible with neutron induced reactions alone.

The European Activation System (EASY), which is being developed and improved by UKAEA Fusion, Culham, Great Britain [Su98, Fo01], is a package consisting of the FISPACT inventory code and the European Activation File (EAF) as a data base. EASY also includes files and routines for SCPR calculation as mentioned above.

Within a task of the European Fusion Technology Programme, integral validation experiments for EASY have been carried out using a neutron source which employs a 19-MeV deuteron beam impinging on a saturation thick beryllium target. The free neutrons are produced in this source mainly by deuteron stripping and, to a lesser extent, deuteron breakup. Neither of these nuclear processes has any resonance features. As a consequence, the neutron spectrum, i.e. the yield as a function of neutron energy, is a smooth continuum ('white' spectrum), in contrast to the resonant fusion reaction T(d,n)^{4}He with its emission of almost monoenergetic neutrons of about 14 MeV.

The advantage of a white spectrum in validating nuclear data for fusion reactor applications lies in the fact that the spectrum in a fusion reactor consists of a line ('peak') at 14 MeV and a flat continuum 'tail' towards lower energies, due to neutron scattering on the reactor materials. T(d,n)^{4}He neutrons produced in laboratory devices (neutron generators) usually do not have this scattering continuum. Adding this continuum artificially by arranging scattering material at the source device is possible in principle, but it would decrease the achievable neutron flux on the sample. Therefore, experiments on those devices test the cross section data essentially at 14 MeV neutron energy, which is very important but not sufficient by itself. Our experiments, on the other hand, give about equal weight to all neutrons throughout the MeV range and are thus complementary to those performed with 14 MeV neutron sources. Moreover, with our method the flux density on the sample can be as high as 1.7×10^{11} n cm^{-2} s^{-1}, higher than with almost any existing T(d,n) neutron generator. The upper neutron energy limit of our source is close to 20 MeV, which also is the upper limit of EAF data. The spectrum of the d-Be source and a typical fusion reactor spectrum are shown in Fig. 2.

The measurable activity of a product nuclide at a given time after a given irradiation of a given sample depends on the reaction cross section and on the decay data, i.e., half lives, branching ratios etc. The decay data are generally much more accurately known than the neutron energy dependent reaction cross sections, $\sigma(E_n)$. The EASY validation experiments, therefore, constitute tests mainly of the cross sections contained in EAF. They are denoted integral experiments because the measured quantity is not $\sigma(E_n)$ but the reaction rate $\int\varphi(E_n)\sigma(E_n)\mathrm{d}E_n$, where $\varphi(E_n)$ is the spectral or differential neutron flux density. They are 'integral' also in the sense that multi-pathway production of the same product occurs frequently.

The EU program task emphasizes investigations on the actual engineering materials of interest in the fusion programme. Activation experiments on such alloys or composite materials have a twin character. They serve for benchmarking (verifying) the activation cross section data of EAF (or any other evaluated data library) with respect to the major constituent elements of a sample. In addition, however, the experiments have turned out to be a very sensitive method of detecting impurities in the material, provided that these yield suitable γ-ray emitting activation products. The sensitivity may well surpass that of chemical or X-ray fluorescence analyses. The quantitative determination of such an impurity can, of course, only be as accurate as the pertinent cross section is known. In practice it is sometimes difficult to decide whether a calculation-experiment discrepancy for a low-level impurity should be interpreted as indicating an incorrect cross section, or rather a concentration of the target nuclide target differing from the material specification or the result of the chemical analysis. An interesting example of the trace analysis capability of our experiments is Nb-92m, a product of the ^{92}Mo(n,p) or the ^{93}Nb(n,2n) reaction (see Sect. 4.2, 4.5 below). With its half life of 10.15 d, it is easily detected. Its presence points to a molybdenum or/and niobium content of the sample material and proves that there will also be the product Nb-92g. This is a very long lived (3.6×10^7 a) γ emitter, which could never be detected directly in experiments of the kind described (see Conclusions section).

Our experiments are limited to γ ray emitting activation products. The fact that γ radiation is emitted at discrete photon energies (spectral lines) specific to each nuclide, together with the high energy resolution offered by semiconductor γ ray detectors, means that a multitude of product nuclides can be quantitatively and independently determined from the same sample at the same time. Also, γ radiation may be considered the most important, because most unwelcome, effect of induced radioactivity. Nevertheless, β activity not accompanied by γ emission is by no means unimportant. The cross sections of reactions yielding such products require experimental verification as well. While β electron or positron spectrometry would hardly be able to separately quantify several source nuclides in the same sample, at least summary tests are possible by measuring the total β radiation power from activated samples. Such decay heat experiments are being conducted, e.g., at ENEA, Frascati, Italy, within the same European programme task.

The present report describes our experiments on vanadium alloys, copper, nickel, lithium orthosilicate, Eurofer-97 steel and tungsten. For the vanadium alloys results, calculation-over-experiment (*C/E)* ratios referring to an older version of the cross section file, EAF-97, were published earlier [Mö98]. The other results were documented earlier in unpublished reports of the EFF-DOC series. The present report exhibits some differences from those, due to corrections of mistakes and, in some cases, re-evaluations or more complete evaluations of the experimental raw data with improved procedures.

2 EXPERIMENTAL METHOD

2.1 Neutron source

The white neutron source, shown schematically in Fig. 1, consists of a block of beryllium metal which is irradiated by a 19 MeV deuteron beam from the Karlsruhe Isochronzyklotron (KIZ). This type of source had been used earlier by S. Cierjacks with deuterons of higher energy from the same cyclotron. The beryllium thickness along the beam direction is 12 mm, more than the range of 19 MeV deuterons. Since the neutrons originate in direct reactions as mentioned above, they are emitted in a narrow forward-peaked directional distribution. KIZ is a fixed-energy cyclotron with a deuteron extraction energy of 52 MeV. For irradiation at 19 MeV, the target has to be positioned at a suitable radius within the cyclotron magnet gap ('internal' target). This results in certain limitations of the method, that could, in principle, be overcome if an extracted 19 MeV deuteron beam were available.

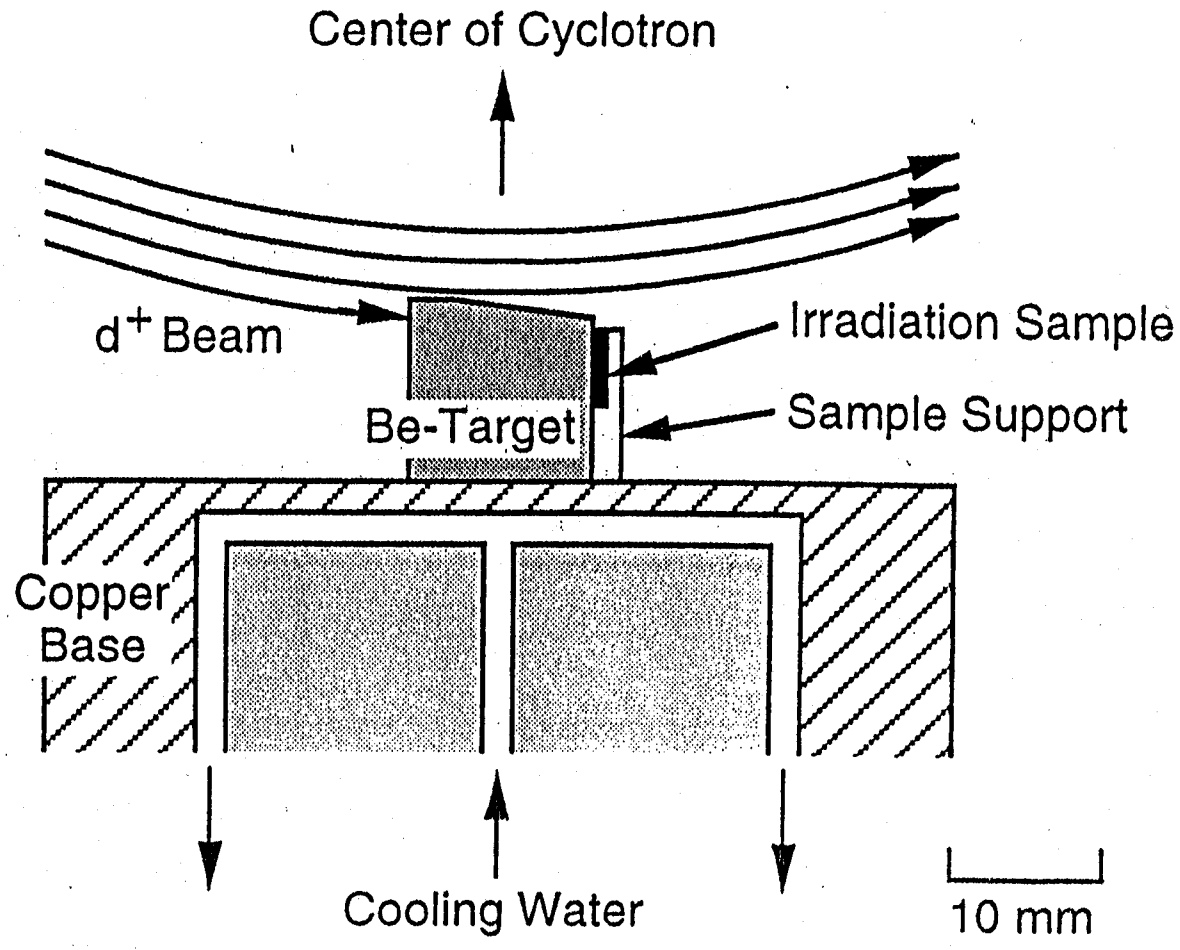

Fig. 1 Deuteron-beryllium neutron source, schematic

E.g., the activation sample cannot be positioned in the target device symmetrically with respect to the beam forward direction, but only shifted to one side (see Fig. 1). This means that about 50% of the produced neutrons are lost, and that the fraction of neutrons hitting the sample, i.e., the neutron

fluence on the sample per unit of deuteron beam charge, is very sensitive to the exact sample position in the device.

The deuteron beam current on target was typically around 10. . .12 μA. This resulted in a neutron flux density of about 1.5×10^{11} $cm^{-2}s^{-1}$ averaged over a 10mm × 10mm sample.

2.2 Neutron spectrum

For meaningful comparisons of the experimental results with calculations, the neutron spectrum of the source needs to be known. For a direct-reaction source of the present type, there is no accurate way to calculate this spectrum. Therefore, it must be measured. The necessity of using an internal target leads to difficulties also in this respect, because the iron pole pieces of the cyclotron above and below at close distance represent a huge quantity of scattering material, so that the neutron spectrum is strongly space dependent and must be measured at a location very close to the source to be realistic. This means that electronic detectors, e.g., a scintillation detector with a photomultiplier tube, cannot be used to measure the spectrum because of the strong magnetic field and radiofrequency noise. Attempts were made to employ a small plastic scintillator together with either an avalanche photo diode (APD), which can be expected to be much less sensitive to external fields than a photomultiplier, or with a long light pipe so that the photomultiplier could be located at some distance from the cyclotron. However, the APD turned out to be destroyed quickly by neutron damage, and the transmission and amplitude resolution of light pipes was found far insufficient[Mö97].

The only feasible way to measure the spectrum was multifoil activation. This was used very successfully, as described in detail in Ref.[Ma99]. However, this method is naturally limited in precision, because the spectrum has to be obtained from a set of measured reaction rates by a numerical unfolding procedure. The resulting spectrum is shown in Fig. 2 and Tables 2-1 to 2-3. It is estimated to be accurate to within ±10% in the energy range from about 10 keV upward. At the low-energy end, however, the accuracy is poorer. The fluctuations seen in Fig. 2 at about 100 eV and lower are obviously an artifact of the unfolding procedure. Consequently, our neutron source is not really suitable for verifying reaction cross sections that are important in the low energy range, i.e., (n,γ) reactions. These reactions, however, can be of importance in the activation of fusion reactor materials. For their experimental validation, use of a fission reactor or similar neutron field is recommended.

The activation foils used in the spectrum measurement had dimensions of 5mm × 5mm. The samples used in the activation experiments described below, however, were mostly 10mm × 10mm, and in one case circular with 10mm diameter. Given the strong space dependence of the flux, spectra to be used in calculations for these samples were derived from the original unfolding result by Monte Carlo calculations[Ma99] using the MCNP-4A code[Br93] together with the McDeLi source routine[Wi97]. The spectrum used in the inventory calculations for 10mm × 10mm square samples is given in Table 2-2, and the one for the 10 mm diameter sample in Table 2-3.

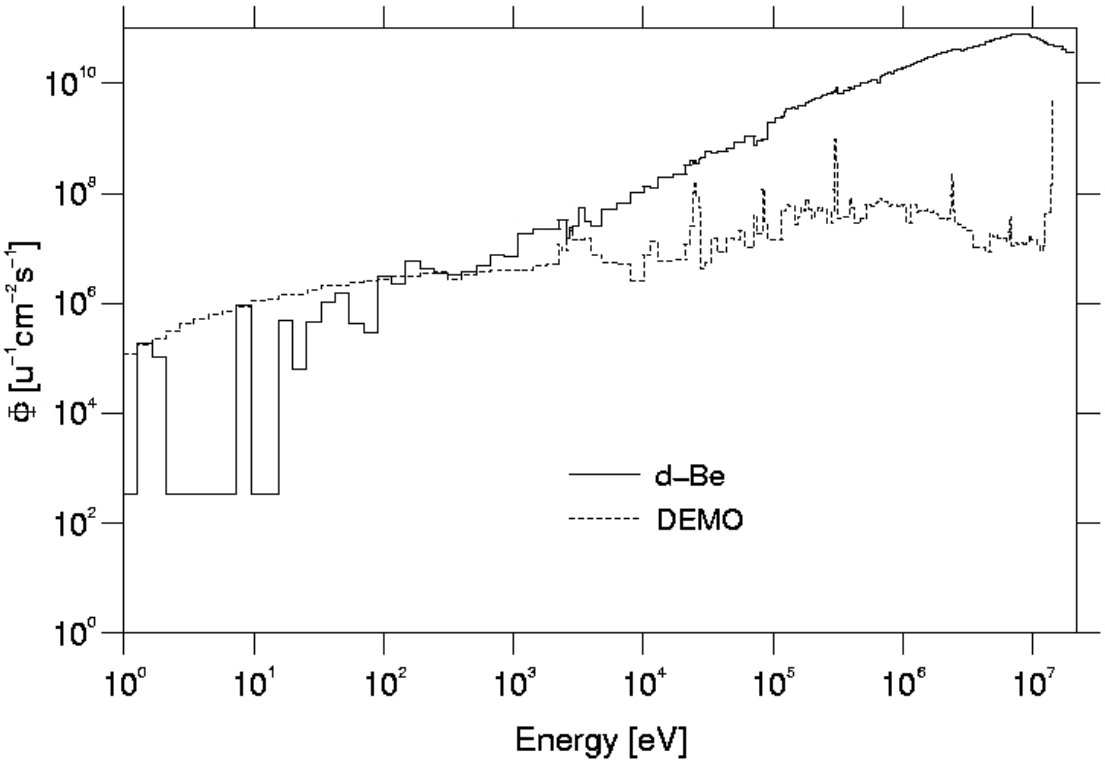

Fig. 2 **Spectra of d-Be neutron source and DEMO reactor (at first wall) in neutrons per unit lethargy**

2.3 Sample preparation

In each experiment, either a single sample or a stack of two different samples was activated. Simultaneous activation of two samples means better exploitation of cyclotron beam time and also has advantages with respect to fluence determination problems (see below). The metallic samples (vanadium alloys, copper, nickel, Eurofer steel and tungsten) were always of square shape and 10mm × 10mm size, with thickness between 0.6 and 1.5 mm. The Li orthosilicate sample was a disc of 10mm diameter and 1.5mm thickness. All monitor foils and stopping foils mentioned in the following always had the same shape and size as the associated sample.

In every case, the sample or samples, as described below with each experiment, were stacked interspersed with 25µm Ni monitor foils. On the upstream side of each sample (in certain cases also of the monitor foils), a 0.1mm graphite stopping foil was inserted to prevent the implantation of activated nuclei from the upstream foil or sample into the downstream one. Without such stopping foils, the gamma rays from, e.g., Co isotopes in case of a preceding Ni monitor foil, or Na-24 in case of a preceding Al foil, could readily be detected in the activated sample. The stopping foil safely prevented this contamination.

Table 2-1 VITAMIN-J group boundaries in MeV

1.96403E+1	1.73325E+1	1.69046E+1	1.64872E+1	1.56831E+1	1.45499E+1
1.45499E+1	1.41907E+1	1.38403E+1	1.34986E+1	1.28403E+1	1.25232E+1
1.22140E+1	1.16183E+1	1.10517E+1	1.05127E+1	1.00000E+1	9.51229E+0
9.04837E+0	8.60708E+0	8.18731E+0	7.78801E+0	7.40818E+0	7.04688E+0
6.70320E+0	6.59241E+0	6.37628E+0	6.06531E+0	5.76950E+0	5.48812E+0
5.22046E+0	4.96585E+0	4.72367E+0	4.49329E+0	4.06570E+0	3.67879E+0
3.32871E+0	3.16637E+0	3.01194E+0	2.86505E+0	2.72532E+0	2.59240E+0
2.46597E+0	2.38513E+0	2.36533E+0	2.34570E+0	2.30693E+0	2.23130E+0
2.12248E+0	2.01897E+0	1.92050E+0	1.82684E+0	1.73774E+0	1.65299E+0
1.57237E+0	1.49569E+0	1.42274E+0	1.35335E+0	1.28735E+0	1.22456E+0
1.16484E+0	1.10803E+0	1.00259E+0	9.61672E-1	9.07180E-1	8.62936E-1
8.20850E-1	7.80817E-1	7.42736E-1	7.06512E-1	6.72055E-1	6.39279E-1
6.08101E-1	5.78443E-1	5.50232E-1	5.23397E-1	4.97871E-1	4.50492E-1
4.07622E-1	3.87742E-1	3.68832E-1	3.33733E-1	3.01974E-1	2.98491E-1
2.97211E-1	2.94518E-1	2.87246E-1	2.73237E-1	2.47235E-1	2.35177E-1
2.23708E-1	2.12797E-1	2.02419E-1	1.92547E-1	1.83156E-1	1.74224E-1
1.65727E-1	1.57644E-1	1.49956E-1	1.42642E-1	1.35686E-1	1.29068E-1
1.22773E-1	1.16786E-1	1.11090E-1	9.80365E-2	8.65170E-2	8.25034E-2
7.94987E-2	7.20245E-2	6.73795E-2	5.65622E-2	5.24752E-2	4.63092E-2
4.08677E-2	3.43067E-2	3.18278E-2	2.85011E-2	2.70001E-2	2.60584E-2
2.47875E-2	2.41755E-2	2.35786E-2	2.18749E-2	1.93045E-2	1.50344E-2
1.17088E-2	1.05946E-2	9.11882E-3	7.10174E-3	5.53084E-3	4.30742E-3
3.70744E-3	3.35463E-3	3.03539E-3	2.74654E-3	2.61259E-3	2.48517E-3
2.24867E-3	2.03468E-3	1.58461E-3	1.23410E-3	9.61117E-4	7.48518E-4
5.82947E-4	4.53999E-4	3.53575E-4	2.75364E-4	2.14454E-4	1.67017E-4
1.30073E-4	1.01301E-4	7.88932E-5	6.14421E-5	4.78512E-5	3.72665E-5
2.90232E-5	2.26033E-5	1.76035E-5	1.37096E-5	1.06770E-5	8.31529E-6
6.47595E-6	5.04348E-6	3.92786E-6	3.05902E-6	2.38237E-6	1.85539E-6
1.44498E-6	1.12535E-6	8.76425E-7	6.82560E-7	5.31579E-7	4.13994E-7
1.00001E-7	1.00000E-11				

Table 2-2 Neutrons in each VITAMIN-J group for 10mm×10mm square samples

4.5364e-10	1.0428e-10	1.0818e-10	2.4064e-10	2.4455e-10	1.2352e-10
1.2425e-10	1.2678e-10	1.3028e-10	2.6531e-10	1.3677e-10	1.4137e-10
3.0293e-10	3.2392e-10	3.4257e-10	3.5506e-10	3.6877e-10	3.8197e-10
3.9700e-10	4.1488e-10	4.1454e-10	4.1233e-10	4.0822e-10	3.9852e-10
1.2966e-10	2.5931e-10	3.8071e-10	3.6590e-10	3.5196e-10	3.3871e-10
3.2735e-10	3.1692e-10	3.0371e-10	5.7018e-10	5.2446e-10	4.8599e-10
2.2573e-10	2.1805e-10	2.0569e-10	1.9763e-10	2.0655e-10	2.1255e-10
1.3877e-10	3.4413e-11	3.4336e-11	6.6250e-11	1.3407e-10	1.9627e-10
1.8913e-10	1.8295e-10	1.7737e-10	1.6984e-10	1.6145e-10	1.5441e-10
1.4915e-10	1.4123e-10	1.3590e-10	1.2905e-10	1.2409e-10	1.1762e-10
1.1069e-10	2.0656e-10	8.1190e-11	1.0609e-10	8.9791e-11	8.5051e-11
7.7770e-11	8.1633e-11	7.7024e-11	7.2830e-11	6.5159e-11	5.3198e-11
5.7276e-11	5.7795e-11	5.4613e-11	5.1886e-11	1.0007e-10	9.2135e-11
4.0409e-11	4.2757e-11	7.4308e-11	6.4832e-11	9.7202e-12	3.0909e-12
6.9612e-12	1.7363e-11	3.6018e-11	6.7459e-11	3.0714e-11	2.9490e-11
2.6484e-11	2.7201e-11	2.6348e-11	2.4127e-11	2.3080e-11	2.0276e-11
1.9778e-11	1.9694e-11	1.6949e-11	1.8545e-11	1.7912e-11	1.7025e-11
1.5539e-11	1.2912e-11	3.0512e-11	2.3992e-11	4.4919e-12	3.4912e-12
9.2135e-12	5.0535e-12	1.8942e-11	6.4427e-12	1.0607e-11	8.1376e-12
9.9989e-12	4.0815e-12	6.4418e-12	2.5124e-12	1.4796e-12	1.7447e-12
9.9482e-13	8.5548e-13	2.9887e-12	4.0097e-12	5.5484e-12	4.8567e-12
1.2980e-12	2.0656e-12	2.6517e-12	1.6822e-12	1.3183e-12	3.7369e-13
2.9946e-13	5.4926e-13	2.6146e-13	1.0691e-13	7.7078e-14	3.2648e-13
3.3155e-13	5.8076e-13	5.5002e-13	4.5645e-13	1.7658e-13	1.8934e-13
1.1823e-13	9.2219e-14	8.3572e-14	8.9686e-14	1.0413e-13	1.4939e-13
5.4766e-14	7.9932e-14	7.3936e-15	1.0700e-14	3.8729e-14	2.6669e-14
1.1257e-14	1.5767e-15	1.1840e-14	8.4450e-18	8.4442e-18	2.2869e-14
8.4442e-18	8.4450e-18	8.4433e-18	8.4450e-18	8.4450e-18	2.5631e-15
4.8381e-15	8.4433e-18	8.4442e-18	8.4450e-18	2.4997e-15	8.4450e-18
2.0251e-17					

Table 2-3 Neutrons in each VITAMIN-J group for 10 mm diameter samples

4.5931e-10	1.0579e-10	1.1063e-10	2.4580e-10	2.5211e-10	1.2790e-10
1.2887e-10	1.2823e-10	1.3381e-10	2.7398e-10	1.4051e-10	1.4721e-10
3.0839e-10	3.3267e-10	3.5288e-10	3.6327e-10	3.7807e-10	3.8955e-10
4.1017e-10	4.2430e-10	4.2314e-10	4.2176e-10	4.1809e-10	4.0642e-10
1.3308e-10	2.6797e-10	3.9285e-10	3.7376e-10	3.6149e-10	3.4698e-10
3.3878e-10	3.2317e-10	3.1445e-10	5.8896e-10	5.4157e-10	4.9993e-10
2.3383e-10	2.2549e-10	2.1796e-10	2.0510e-10	2.1534e-10	2.2007e-10
1.4553e-10	3.5176e-11	3.4358e-11	6.8570e-11	1.4068e-10	2.0505e-10
1.9819e-10	1.8953e-10	1.8611e-10	1.7854e-10	1.7041e-10	1.6353e-10
1.5475e-10	1.4431e-10	1.4615e-10	1.3713e-10	1.2950e-10	1.2325e-10
1.1630e-10	2.1527e-10	8.6497e-11	1.1369e-10	9.2717e-11	9.0779e-11
8.0399e-11	8.5658e-11	8.2161e-11	7.6648e-11	7.0635e-11	5.5228e-11
6.2140e-11	6.0342e-11	5.8046e-11	5.4847e-11	1.0578e-10	9.7394e-11
4.2716e-11	4.5197e-11	7.8549e-11	6.8533e-11	1.0275e-11	3.2673e-12
7.3585e-12	1.8354e-11	3.8074e-11	7.1309e-11	3.2468e-11	3.1173e-11
2.7995e-11	2.8754e-11	2.7852e-11	2.5504e-11	2.4397e-11	2.1434e-11
2.0907e-11	2.0818e-11	1.7916e-11	1.9604e-11	1.8934e-11	1.7997e-11
1.6426e-11	1.3649e-11	3.2253e-11	2.5362e-11	4.7483e-12	3.6904e-12
9.7394e-12	5.3419e-12	2.0023e-11	6.8104e-12	1.1212e-11	8.6021e-12
1.0570e-11	4.3144e-12	6.8095e-12	2.6558e-12	1.5640e-12	1.8443e-12
1.0516e-12	9.0431e-13	3.1593e-12	4.2385e-12	5.8650e-12	5.1339e-12
1.3721e-12	2.1835e-12	2.8031e-12	1.7783e-12	1.3935e-12	3.9502e-13
3.1655e-13	5.8061e-13	2.7638e-13	1.1302e-13	8.1477e-14	3.4512e-13
3.5047e-13	6.1391e-13	5.8142e-13	4.8250e-13	1.8666e-13	2.0014e-13
1.2498e-13	9.7483e-14	8.8342e-14	9.4805e-14	1.1007e-13	1.5792e-13
5.7892e-14	8.4494e-14	7.8156e-15	1.1311e-14	4.0939e-14	2.8191e-14
1.1900e-14	1.6667e-15	1.2516e-14	8.9270e-18	8.9261e-18	2.4174e-14
8.9261e-18	8.9270e-18	8.9252e-18	8.9270e-18	8.9270e-18	2.7093e-15
5.1143e-15	8.9252e-18	8.9261e-18	8.9270e-18	2.6424e-15	8.9270e-18
2.1407e-17					

Household Al foil of 20µm thickness was used to wrap the entire stack. The wrapping was always done in such a way that there was only a single Al foil layer on the upstream side. The package was then clamped to the Be target block by a simple screw device, using, whenever the available space in the holder permitted, a steel or Al plate between the screw and the package for pressure distribution. A schematic example is shown in Fig. 3.

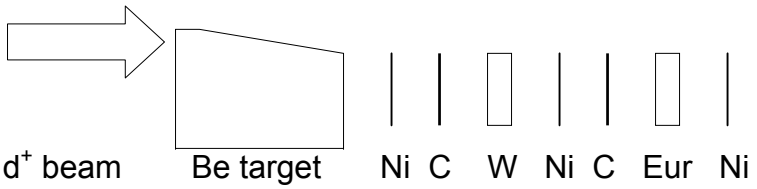

Fig. 3 **Example of activation sample pack, schematic**

Ni	Fluence monitor foils, 25 µm nickel
C	Stopping foils, 100 µm graphite
W, Eur	Activation samples, 0.5 ... 1.5 mm

(Wrapping foil and clamp device not shown)

2.4 Fluence determination

In addition to the spectral shape, the neutron fluence (the time integral of the flux density) applied in an irradiation must be known if the inventories predicted by calculation are to be verified in an absolute sense.

In experiments at 14 MeV neutron sources, it is customary to use activation foils of, e.g., Al, Ni or Nb for neutron fluence measurement. This method relies on the rather precisely known cross sections of certain activation reactions near 14 MeV. With the present white spectrum this was not considered useful because of insufficient certainty about the cross sections. However, we have regularly used the nickel monitor foils mentioned above for measuring the relative fluence decrease across a sample or stack of samples. This decrease is not due to neutron interactions in the sample (because the mean free path of fast neutrons is much longer than the sample thickness), but to the geometry of neutron emission from the effective target volume within the Be block. That volume has lateral dimensions of a few millimeters, and the neutrons are emitted from it in a divergent way. The fluence decrease is typically about 10% per mm of sample stack thickness. Ni is a favourable monitor because it offers two suitable reactions, $^{58}Ni(n,p)^{58}Co$ and $^{58}Ni(n,2n)^{57}Ni$, having threshold neutron energies of 0.4 and 12.4 MeV respectively. The fluence decrease factor was evaluated both from the Co-58 and the Ni-57 γ ray counts, and no difference between the two activation products was found in this respect.

This indicates that the fluence decrease is essentially independent of neutron energy, in agreement with the above reasoning.

For absolute fluence determination, it was originally attempted to use the deuteron beam current on the target directly as a measure of flux density and thus the accumulated charge as a measure of fluence, employing the calibration factor in neutrons per cm^2, second and microampere obtained from the spectrum measurement. This worked well in the first few experiments including the vanadium experiment (see below). In the next experiment, however, it produced *C/E* ratios that suggested an incorrect fluence assumed in the calculation, resulting in an erroneous common factor modifying all of the *C/E*. The likely reason of the discrepancy with the former experiments is differences in the irradiation geometry. It is difficult to ensure precise reproduction of the sample position in the target device, and moreover, the position of the deuteron beam spot on the target front surface is somewhat variable from one experiment to the next because of magnetic remanence effects in the cyclotron. For all the later experiments, therefore, other ways of fluence determination had to be found, that will be described under the individual experiments.

2.5 Time dependent flux

For the discussions in this and later sections, a nomenclature of the various time points and time intervals in an activation experiment is required. Let t_B and t_E denote respectively the beginning and end time of the activation, $T_A = t_E - t_B$ the activation duration, t_M the start of a gamma spectrum registration, $T_c = t_M - t_E$ the cooling time and $T_{1/2}$ the half life of a radionuclide.

The well known relationship between the total neutron flux density Φ and the activity at irradiation end, $A(t_E)$, is

$$A(t_E) = \sigma\Phi\,(1 - \exp(-\lambda T_A)), \qquad (1)$$

where σ is the energy-integrated cross section and $\lambda = \ln 2/T_{1/2}$ the decay probability of the nuclide. Eq.(1) holds if Φ is constant during the irradiation or, with Φ being the average flux, if $T_A << T_{1/2}$.

A constant flux during irradiation can usually be provided to a good approximation in fission reactors, but accelerator-based neutron sources typically have temporal variations of the flux and/or more or less frequent and extensive beam-off times. The second of the above conditions, $T_A << T_{1/2}$, cannot be fulfilled if nuclides of short and long half lives are to be investigated in the same sample and T_A is chosen long enough to produce sufficient activity of the long lived species. Therefore, we generally have to take into account the variations of $\Phi(t)$ about its average. This demands that some quantity proportional to $\Phi(t)$ be recorded with a time resolution better than the shortest half life of interest. In practice, we have used the deuteron beam current on the target as registered by a current-to-frequency converter and a scaler (Ortec model 974) controlled and read out by a personal com-

puter. The time resolution, i.e. the interval of current integration, was selected at 20 to 60 seconds, depending on the shortest half life of interest.

2.6 Gamma spectrometer

2.6.1 Apparatus

The gamma spectrometer consists of a high purity germanium (HPGe) detector, EG&G-Ortec model GEM-25185-P, of 30% relative efficiency.[1] The crystal dimensions are 54.5 mm diameter and 64.4 mm length. The detector is connected via a hybrid preamplifier (Ortec 237P) and a shaping amplifier (Ortec 672) to a personal-computer-based multichannel analyzer using an Ortec 919 analog-to-digital cnverter (ADC). The block scheme is shown in Fig. 4. The settings used were:

Detector voltage	+2000 V
Pulse Shaping	triangular, 6 µs
Pole-zero cancellation	automatic
Base line restoration rate	automatic
number of channels	4096

The amplifier gain was adjusted to yield a conversion gain of about 0.5 keV/channel, so that the gamma energy range of each spectrum was about 0 . . . 2 MeV. The energy resolution (full width at half maximum) of photo peaks was found to be about 1.7 keV or slightly over 3 channels. The 4096 channel memory, therefore, offered adequate digital resolution.

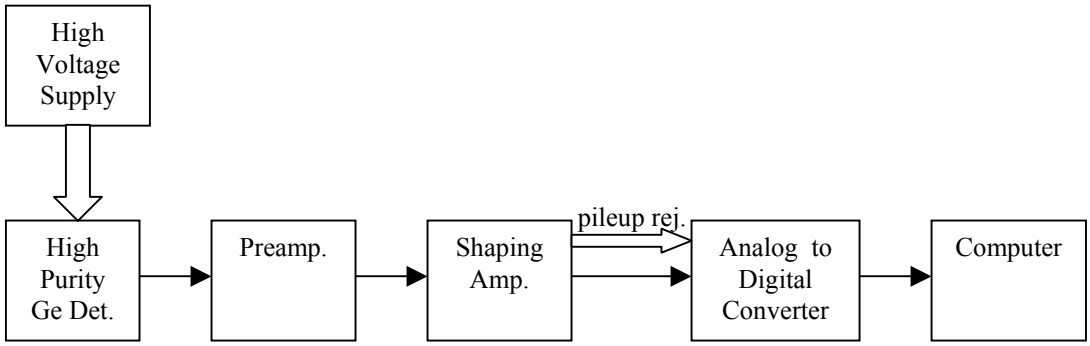

Fig. 4 Block diagram of gamma spectrometer electronics

The dead time behaviour in this simple electronic chain is dominated by a single component, the ADC. Due to the presence of relatively long lived nuclides, the overall counting rate during each measurement is approximately constant. Under these conditions, correction for dead-time losses can

[1] i.e. the absolute detection efficiency for 1332 keV photons from a point source located on the cylinder axis of the detector at 25 cm source-detector distance is 30% of that of a 3 inch by 3 inch NaI(Tl) scintillator.

be made in the standard way by using, in analyzing the recorded spectra, the ‘live’ time as recorded in a separate register and not the ‘real’ or elapsed time of the measurement [Mö94.

The Ortec 672 amplifier together with the Ortec 919 ADC performs pile-up rejection by creating an artificial dead time whenever a distorted pulse shape is detected. Combined with this feature, a relatively harmless defect of one of the integrated circuits (IC) in the preamplifier led to a randomly occurring problem, which made a number of recorded γ spectra worthless until it was noticed and identified. The IC defect caused a slight undulation superimposed on the trailing edge of the pulses, the undulation amplitude strongly increasing with the pulse amplitude. Thus, the trailing edge of larger pulses occasionally would go through a minimum and then rise again, which would erroneously trigger the pile-up rejection circuit, while small pulses would be transmitted without problem. This meant a temporary reduction of the detection efficiency in a γ energy dependent way. The effect was discovered only by the particularly small 1461 keV K-40 background peak in one spectrum. A retrospective analysis of known peaks above 1 MeV in other spectra then showed that the effect had occurred in a fast varying manner, so that, e.g., a calibration spectrum could not even be guaranteed to be valid in analyzing a sample spectrum taken immediately afterwards. After identifying this effect and replacing the faulty preamplifier IC, the background 1461 keV peak count rate has been regularly monitored as a precaution.

A shield enclosing the detector and gamma ray source was built, in the shape of a horizontal tunnel of about 20 cm internal width and height and 80 cm length, from standard lead blocks of 5 cm thickness. A 1 cm copper liner serves as a mechanical support for the tunnel roof and also for suppressing the Pb X-ray fluorescence radiation. No particular attention was paid to the age or irradiation history of the lead and copper parts. This explains why some gamma lines from Bi isotopes (contained in the lead) and Co-60 (contained in the copper) are observed in the background spectrum of the spectrometer. However, with regular re-measurements of this background spectrum and peakwise background subtraction in analyzing the sample spectra (see next section) this does not notably impair the accuracy of results, except for the sensitivity to very weak activities. The total background count rate (in the gamma ray energy range up to 2 MeV) is close to 5 counts/s.

To allow for a certain range of γ ray source intensities, five fixed positions for the sample holder at different distances from the detector are provided by holes at the bottom of the shield, into which fitting pins on the sample holder can be inserted. This ensures easy and accurate reproducibility of the sample-detector geometry. The sample-detector distances are about 5, 10, 20, 40 and 70 cm. The sample holder is designed so that it can either take a Eu-152 calibration γ ray source or an activated sample. Either kind of sample is held in an opening of a thin aluminium plate (in case of the activated samples by putting them on a strip of thin adhesive film), so that there is little additional scattering material near the radiation source and practically none behind it.

2.6.2 Energy calibration

The background lines at γ ray energies E_γ = 511 keV (positron-electron annihilation, probably due to cosmic ray muon decay events), 1461 keV (K-40, contained in building materials) and 1770 keV (Bi-207, from the Bi impurity of the lead shielding) are convenient energy calibration marks. The spectrometer response is so exactly linear that a straight line using just the 511 and 1461 keV peak maximum channels gave an energy calibration that permitted identification of any other gamma ray peak in the spectra.

2.6.3 Efficiency calibration

The absolute detection efficiency ε, i.e., the number of full-energy peak counts per photon emitted from the sample, depends on the measurement position selected (see above) and on the gamma energy. For each position used, therefore, γ lines at various energies from one or several samples of known activity (calibration sources) must be recorded to establish a calibration function $\varepsilon(E_\gamma)$ for that position. As gain factors etc. of electronic components may be subject to some drifts, such calibration should be repeated shortly before or after any sample measurement.

Our standard procedure has been to take a calibration spectrum with a certified Eu-152 γ ray source. This yields calibration points at 11 conveniently spaced energies from 121 to 1408 keV. Least squares fits of the four functions

$$\ln\varepsilon = a_0 + a_1 E_\gamma + a_2 E_\gamma^{-1} \quad (2)$$

$$\ln\varepsilon = a_0 + a_1 E_\gamma + a_2 E_\gamma^{-1} + a_3 E_\gamma^{-2} \quad (3)$$

$$\ln\varepsilon = a_0 + a_1 E_\gamma + a_2 E_\gamma^{-1} + a_3 E_\gamma^{-2} + a_4 E_\gamma^{-3} \quad (4)$$

and

$$\ln\varepsilon = a_0 + a_1 E_\gamma + a_2 E_\gamma^{-1} + a_3 E_\gamma^{-2} + a_4 E_\gamma^{-3} + a_5 E_\gamma^{-4} \quad (5)$$

to the set of net peak areas were then calculated, and the one with the minimum χ^2 per degree of freedom (a measure of the goodness of fit) was selected for use. This was always either Eq. (3) or (4). It yielded a calibration table which can be used with an estimated uncertainty of ±2% in the range of about 120 to 1500 keV.

The calibration method with a multi-line source such as Eu-152 is, in principle, subject to certain systematic errors because some of the γ lines are emitted in a coincident way. If both of the coincident photons interact with the detector, they will be recorded as a single pulse not located in either of the two full energy peaks, so that a counting loss results. This could be avoided by the more complex and time consuming way of taking many separate calibration spectra with a set of single-line sources. (Similar systematic errors can, of course, occur in measurements of an activated sample emitting coincident photons.)

The probability of coincident detection of the two photons varies as the square of the solid angle subtended by the detector at the source. With the dimensions mentioned in section 2.6.1, the maximum solid angle in our spectrometer is only 0.66 sr or about 5% of a full sphere (4π sr). Therefore, the coincidence related error was considered negligible in our experiments in view of the other experimental uncertainties.

2.7 Gamma spectra acquisition

Usually, the samples were removed from the target device as soon as possible after the activation. The first gamma spectrum measurement from an activated sample could then be started at $T_c \approx 15$ min. Following a traditional rule of thumb, more spectra from the same sample were then taken after cooling time intervals that increased each time by roughly a factor of 5, e.g., after about 1 h, 5 h, 1 day, 1 week, 1 month, 5 months. In this way, γ emitters of any half life not too far outside this range of cooling times show up in at least one of the recorded spectra. The duration of each spectrum registration was usually about 50 . . . 100% of T_c, but not longer than a few days. In case of two samples activated simultaneously, usually one was more interesting than the other with respect to short lived products, and this one was then given priority for the first measurement.

This complete scheme was applied in the experiments whenever there was interest to measure and analyze as many gamma emitting nuclides as possible in a sample. In some experiments, however, fewer spectra were taken, as noted below, either because of technical difficulties or because the interest was limited to a few selected nuclides.

Occasionally, a background spectrum without any sample was recorded and checked for consistency with former ones. Whenever any radioactivity in the sample prior to irradiation was deemed possible, the background spectrum was taken with the unirradiated sample in place. These background spectra were then used for background subtraction in the analysis of other spectra (see below).

2.8 Gamma spectra analysis

2.8.1 General procedure

The commercial software used for accumulating the γ ray spectra (EG&G-Ortec GammaVision™) also offers automatic spectrum analysis functions. These features are useful in case of series measurements of samples of one kind, where only some well known peaks of sufficient statistical accuracy are of interest. In most of our experiments, however, any unknown small peak in a spectrum may indicate an unexpected impurity activation product and should, therefore, be analysed. For such purposes we have, after some experience, preferred a 'manual' analysis of the spectra (using a number of simple Fortran programs of our own) mainly for the following reasons:

- The automatic recognition of peaks, i.e. setting of 'regions of interest' in the spectrum, was found not reliable in cases of poor statistical accuracy.
- Subtraction of a background spectrum can be done within the automatic procedure only channelwise. This presupposes very precise equality of the energy calibration curves of the two spec-

tra, and even then leaves a difference spectrum with small peaks that are difficult to interpret because they may either be due to real γ rays or just artifacts of counting statistics. In the manual procedure a background spectrum can be subtracted peakwise, i.e., the differences of the net count rates of associated peaks in the two spectra are calculated, which is a much more robust method.

- The automatic procedure always analyzes one spectrum file independently of others, taken, e.g., from the same sample at earlier or later cooling times. However, following the time behaviour of a peak in the spectrum is often instrumental in confirming or excluding a candidate nuclide. This function is not provided by the GammaVision software.
- The original library of γ energies and decay data supplied with GammaVision is too large to be used directly in the automatic procedure. The user has to define a subset, i.e., to decide prior to the analysis which γ emitting nuclides may be present. This introduces some arbitrariness. It appears safer to identify candidate nuclides in a non-automatic step using the Ortec Nuclide Navigator software.

2.8.2 Determination of specific activities

Specific activities of the product nuclides are inferred from the full-energy peak net counting rates of one or several of their characteristic γ spectral lines. After finding the net areas with statistical uncertainties of any candidate peaks, these areas are divided by the live time of the measurement to obtain mean counting rates a. The counting rate at t_M is obtained from a by multiplying with a factor

$$z_M = \lambda T_M / (1\text{-}\exp(\lambda T_M)) \tag{6}$$

where T_M is the 'real' (not the 'live') duration of the spectrum measurement. This decay-during-acquisition correction is important whenever the half life is not much longer than T_M .

The specific activity at t_M of the nuclide in question is

$$A_{sp}(t_M) = a\, z_M / (m\, k_d(E_\gamma)\, \varepsilon(E_\gamma)\, I_\gamma) \tag{7}$$

where m is the sample mass, $k_d(E_\gamma)$ the γ ray attenuation factor for the sample material and thickness, $\varepsilon(E_\gamma)$ the absolute efficiency as defined above, and I_γ the γ ray intensity, i.e. the number of photons of the specific energy emitted per decay. The I_γ data for our analyses were taken from Firestone et al.[Fi96]. If a nuclide has more than one γ line of useful energy and intensity, $A_{sp}(t_M)$ can be determined from each line independently. In these cases, the $A_{sp}(t_M)$ given in the results tables below is the average, weighted with the statistical uncertainties.

A problem arises when two isobaric nuclides decaying to the same daughter are present, e.g., Sc-48(β^-)Ti-48 and V-48(β^+)Ti-48. In such cases, some or most of the γ lines may be common to both of the pathways. For a separate determination of the two products, at least for one them a specific line needs to be analyzed, which typically is of low intensity resulting in poor statistical accuracy. An

alternative way exists if the two half lives differ sufficiently (i.e., at least by about an order of magnitude). Two spectra taken at appropriate cooling times will then give sufficient information to determine either product.

2.8.3 Experimental uncertainty

There are several contributions to the experimental uncertainty of $A_{sp}(t_M)$:

- counting statistics of the individual γ ray line,
- detector efficiency calibration,
- uncertainty of γ ray attenuation in sample (important for the lowest γ energies).
- uncertainty of γ ray intensities (usually very small, and not accounted for in this work).

Further experimental uncertainties are those

- of the target nuclide concentration in the sample,
- of the neutron spectrum and fluence determination,
- for short half lives, limited time resolution of target current registration and uncertainty of cooling time.

These have no influence on the measured but on the calculated specific activities, and so they nevertheless contribute to the uncertainties of the *C/E* ratios.

Some of the experimental uncertainty contributions are individual for each γ ray line, others are common to all lines from the same nuclide, and some are common by magnitude and direction to all results from a given experiment.

In any averaging of results, the rule has been followed to use weights based only on those uncertainty components that are individual to each single result, and to consider the greater of the internal standard deviation (obtained from Gaussian uncertainty propagation) and external standard deviation (weighted scatter of the individual results) as the uncertainty of the mean. This is then combined with the covariant contributions to give a final uncertainty (which has usually been rounded). All uncertainties quoted are to be understood as one standard deviation. The minimum experimental uncertainty of our *C/E* ratios is ±10%, the estimated uncertainty of the source neutron spectrum.

Note that there is, in addition to the uncertainties discussed here, a further one which can hardly be quantified, the possibly inhomogeneous distribution of minor constituents in the sample material (see discussion in section 4.1).

3 INVENTORY CALCULATIONS

3.1 EASY-99 calculations

The European Activation System (EASY) [Su98], consisting of the inventory code FISPACT and the cross-section library EAF with associated decay, biological hazard, and transport data, is developed for activation analyses in a fusion environment.

The FISPACT code solves the inventory equations using effective cross-sections collapsed using a given neutron spectrum. The code is able to treat multi-step reactions, the fission of actinides, the transmutation of radioactive nuclides (half-life > 0.5 day) including transmutation to and from isomeric states, and the activation induced by sequential charged particle reactions (SCPR). An inventory calculation with FISPACT requires as an input the neutron flux and spectrum, cross-section and decay data, the chemical composition of the irradiated material, and a specification of the irradiation period. The output of FISPACT includes the inventory of nuclides and activation quantities such as specific activities, dose rates, and decay-heat production. FISPACT is also capable to trace the pathway of reaction-decay chains for the generation of a given nuclide.

The European Activation File (EAF) contains cross-section data of neutron induced reactions for 766 target isotopes between Z=1 and Z=100 for energies up to 20 MeV. The data originate from different sources such as evaluated general purpose data libraries, experimental data libraries, model and systematic calculations, and learned estimations. Accordingly, the uncertainty of the data varies to a large extent. Associated with the EAF is also an uncertainty file for the estimation of data related uncertainties.

The inventory calculations for the present work have been performed with the EASY-99 package. The neutron flux has always been assumed to be constant over the irradiation period. The measured neutron spectrum[Ma99] was processed into the VITAMIN-J 175 group structure which was then used to generate effective cross-sections from the available multi-group EAF library processed in the same group structure assuming infinite dilution.

The detailed chemical compositions of the irradiated materials were taken either from supplier's specifications or from experimental analyses done in connection with the present work (see section 4). The results of the calculations include along with the nuclide inventory, activation quantities, dominant nuclides contributing to the calculated quantities, pathways of dominant nuclides, and uncertainties of calculated quantities.

Activation by SCPR is accounted for by the method of Cierjacks et al. [Ci91,Ci93] implemented in FISPACT. The method relies on the use of so called pseudo cross-sections formed from the secondary charged particle (proton, deuteron, triton, He-3 and alpha) spectrum and the charged particle reaction cross section of the type (x,n) and (x,2n) along with the stopping range of the charged particle. Once the pseudo cross-sections are calculated, they can be treated like effective cross-sections in the inventory calculations. Effects of SCPRs are significant for the activation of low and medium

mass nuclides, where neutron induced charged particle emission is favourable due to low Coulomb barriers. However, the charged particle fluxes are several orders of magnitude lower than the neutron flux, so that the product inventory induced by SCPR is mostly inferior. It can be of practical importance in the cases where a nuclide is generated only by a SCPR path.

Using the pathway analyses the percent contributions of various reaction and decay chains to the production of each nuclide have been determined.

Furthermore, the pathway analysis serves as a basis for the estimation of the uncertainty of the calculated quantities. Data related uncertainties in the calculated quantities are estimated using the uncertainty data file associated with EAF. The uncertainty for the production of a given nuclide is calculated from the error contribution of each pathway leading to its production. Within a pathway the errors are square summed. The uncertainty of a given quantity is obtained by composing the uncertainty of the dominant nuclides contributing to it.

3.2 Accounting for time dependent flux

As discussed in section 2.5, the neutron flux may vary during the activation, and this has to be accounted for in the inventory calculation. In the present work, the EASY calculations were always performed for a 'rectangular' flux, i.e. the mean flux Φ applied in a constant way over the duration T_A. The calculated specific activities, therefore, need to be corrected for the actual time behaviour of the flux. From the recorded beam charge data x_i, i=1,..., n, recorded at the times t_i (see sect. 2.5), a correction factor ψ can be obtained[Mö93] as

$$\psi = \sum x_i \exp(-\lambda(t_E - t_i)) \,/\, (\langle x \rangle \sum \exp(-\lambda(t_E - t_i))) \qquad (8)$$

where $\langle x \rangle = (1/n)\sum x_i$. The factor describes the modification of an activity calculated according to Eq. (1). A Fortran program was written to evaluate ψ for arbitrary decay probabilities λ from the recorded data. The specific activities calculated by EASY were then multiplied by their corresponding ψ. The ψ are given in the results tables below for use in future comparisons of our experimental results with calculations.

4 EXPERIMENTS AND RESULTS

4.1 General remarks

In this chapter, five experiments are described in chronological order of their execution. They were performed between September 1997 and June 2001. In each case four tables are given, containing (1) the activation parameters, (2) the elemental composition of the material, (3) the experimental results proper (i.e. the measured specific activities A_{sp} in Bq per kg of sample material as found at different cooling times), and (4) *C/E* ratios and some other quantities related to or taken from the EASY-99 calculation. The half lives mentioned in the tables are rounded values for orientation only. Note that the uncertainties given for the A_{sp} contain only the counting statistics and, in cases of more than one useful γ line, the scatter of those single results, but not the covariant uncertainty components due to the neutron spectrum (see section 2.2). The uncertainties given here were used for weighted averaging of the *C/E* from different cooling times.

For the calculation-related table, some more explanations are necessary.

- "Exp." and "EASY" denote experimental and calculated results respectively.
- The γ dose rate fraction f_D^* is the highest percent contribution of each nuclide to the total γ dose rate from the sample given by EASY at any of the discrete cooling times investigated. It is meant to give an impression of the practical importance of each nuclide. The true maximum of the γ dose rate fraction will be close to of f_D^* for any product having a halflife within the range of cooling times investigated; however, a nuclide with very short half life may obviously make a much higher percent contribution at some very early cooling time, and a very long lived one correspondingly at a very late cooling time.
- The flux correction factor ψ was defined in section 3.2. It will be required in future comparisons of the experimental results with calculations.
- The *C/E* have been obtained by combining each A_{sp} from the previous table with the EASY-99 result for the same cooling time, taking into account the ψ correction if any. Where several *C/E* for different cooling times were available, the figure given is their weighted average. The experimental uncertainty of the averaged *C/E* and the uncertainty given in the EASY output, based on the EAF uncertainty file, are given separately. The experimental uncertainty given here is the total one including the covariant contributions for the neutron spectrum, target nuclide concentration, etc. *C/E* values in parentheses indicate questionable experimental results. Comments on these are found in the Remarks column or in the text.
- The pathways and their percentages are also quoted from the EASY calculation. Note that, throughout this report, reactions involving the same target, projectile and residual nuclide are not distinguished from each other. E.g., W180(n,t) stands for W180(n,t) + W180(n,nd) + W180(n,2np), etc. The pathway percentages are time dependent wherever one or more branches proceed via radioactive decays. In such cases the percentages at a specified cooling time are quoted. Note also that the quoted pathways are 'generic', i.e., they include any possible channels leading to the ground state of the residual nucleus directly or via isomeric states, except in cases where an isomeric product by itself is measured and reported, e.g., Nb-92m.

Sequential charged-particle induced reactions and (n,γ) reactions are highlighted by boldface letters. For the former, the EASY results are of limited accuracy due to the approximate calculation method mentioned earlier. EASY does not give an uncertainty for these. The (n,γ) results are also uncertain in an absolute sense because of the poorly known low energy flux of our neutron source; nevertheless, the variation among (n,γ) *C/E* values found for different products in the same activated sample, e.g. in case of Eurofer-97, probably indicates problems with at least some of the respective (n,γ) cross sections in EAF.

- Finally, in cases where one generic pathway accounts for 90% or more of the yield, the experimental cross section σ for that generic pathway in our neutron spectrum, $\sigma = \int\varphi(E_n)\sigma(E_n)\mathrm{d}E_n / \int\varphi(E_n)\mathrm{d}E_n$, is given. These values were obtained by dividing the EASY-99 cross section (or sum of isomeric cross sections), as found in the PRINTLIB output, by the *C/E* and multiplying by the percent share of the pathway. Where one or more isomeric branches exist, a mark 'g+m' will be found. The relative uncertainty of σ is, obviously, essentially the same as the experimental relative uncertainty of *C/E*. Note, however, that in case of a strongly discrepant cross section in one of several pathways, the EASY pathway percentages will be incorrect.

The elemental concentrations for each sample are mostly given with uncertainties. However, there is an additional source of uncertainty which cannot be accounted for in a quantitative way, namely, inhomogeneous distribution of a minor alloy or a trace impurity in the material. The chemical analyses are necessarily performed on a sample which is not the activated one; the best that can be done is to cut the analysis sample and the activation sample from the same plate etc. as close as possible to each other. The relative variation of the concentration across the material likely is smaller for higher concentrations than for low ones. In other words, *C/E* obtained on major constituents of a sample are generally more credible than those on minor constituents. Before using any of our experimental results in modifying cross section evaluations, the target nuclide concentration in the experimental sample should always be taken into consideration in that sense.

The symbol < in the result tables reflects target nuclide concentrations that are only known as upper bounds, as shown in the composition tables. The EASY calculation in these cases was usually made assuming a concentration equal to that upper bound.

Generally, the comparison with calculated specific activities has been made only for those product nuclides actually identified in the experiments. This means that, e.g., one or the other overestimation of a cross section in EAF might have gone unnoticed if the actual activity was too low to be detected.

4.2 Vanadium alloys

4.2.1 Description of experiment

Samples of two different vanadium alloys, having nominal compositions V3Ti1Si (subsequently referred to as alloy A) and V5Ti2Cr (alloy B), were activated together as a sandwich according to Table 4-1.

Table 4-1 Activation parameters

	Alloy A	Alloy B
T_A	65.0 h	
Φ	1.444 E11 cm^{-2} s^{-1}	1.599 E11 cm^{-2} s^{-1}
m	0.397 g	0.296 g
Sample shape	square 10mm × 10mm	
Sample thickness	0.75 mm	0.6 mm

The elemental compositions as analyzed by C. Adelhelm et al. at the Materials Research Institute of Forschungszentrum Karlsruhe are given in Table 4-2. The material pieces for chemical analysis were cut adjacent to the activation samples from the same plates. For practical reasons connected with improvement work on the spectrometer, γ spectra were taken only at relatively long cooling times, T_c = 41 d and 115 d for alloy A and 112 d for alloy B. Consequently, only products with relatively long half lives (≥ 3.3 d) were covered in this experiment.

Table 4-2 Elemental composition

Element	Alloy A		Alloy B	
	weight %	± weight %	weight %	± weight %
Al	<0.001		0.0073	0.0016
Si	1.035	0.018	0.118	0.0005
Ti	3.150	0.092	4.885	0.118
Mn	<0.00005		0.0004	0.0001
Cr	<0.001		2.036	0.014
Fe	0.036	0.001	0.057	0.006
Ni	0.0043	0.0001	0.0031	0.0002
Zn	<0.001		<0.001	
Zr	0.0176	0.0019	0.0088	0.0011
Nb	0.0014	0.00005	0.0119	0.00005
Mo	<0.005		<0.005	
Pb	<0.002		<0.01	
V	balance		balance	

The fluence on either sample was derived using the relationship between deuteron charge and neutron fluence as obtained from the neutron spectrum measurement, with modifying factors describing the geometrical flux decrease as found by the monitor foils.

4.2.2 Results and discussion

The results are given in tables 4-3 to 4-5. For some specific product nuclides we note the following:

Sc-47 results from four different reaction paths, so that it is difficult to draw definite conclusions about the EAF cross sections. In a former comparison [Mö98] with EAF-97, *C/E* ≈ 6 had been found for Sc-47. Further comparison with activation results obtained by Seidel et al.and Pillon et al. in 14-MeV neutron fields had then revealed that the V51(n,nα) cross section in EAF-97 was strongly overestimated.

For Mn-54 we have conflicting results from the two samples. This is believed to indicate a deviating iron impurity concentration in at least one of the materials. We have no way of deciding which of these *C/E* is more credible. A result from a sample in which iron is not only an impurity is found in Table 4-19.

The Co isotopes, produced from Ni, are all underestimated. A later dedicated experiment on pure nickel (see next section) gave *C/E* much closer to unity. This may indicate that also the Ni impurity concentrations in Table 4-2 are incorrect, which would be a common error of similar direction and magnitude in the two chemical analyses. Such an error cannot be excluded, considering that both of the analyses were performed at about the same time and using the same methods.

Cr-51 in alloy A results mainly from a sequential charged particle reaction, ^{51}V(p,n). The uncertainty given by EASY is unrealistically small.

Table 4-3 Vanadium alloys, experimental results

Product	≈ $T_{½}$	Alloy A				Alloy B	
		T_c = 984 h = 41 d		T_c = 2755 h ≈ 115 d		T_c = 2683 h ≈ 112 d	
		A_{sp}	±	A_{sp}	±	A_{sp}	±
		Bq/kg	%	Bq/kg	%	Bq/kg	%
Sc46	84 d	**9.30 E6**	1	**5.06 E6**	0.2	**8.55 E6**	1
Sc47	3.3 d	**1.32 E5**	9				
Cr51	28 d	**3.21 E5**	23	**4.27 E4**	29	**5.86 E6**	0.6
Mn54	312 d	**6.55 E4**	17	**5.30 E4**	5	**4.40 E4**	5.8
Co57	272 d	**1.26 E5**	7	**9.59 E4**	1.6	**1.41 E5**	1.4
Co58	71 d	**7.66 E5**	2.4	**3.79 E5**	1	**5.39 E5**	1
Co60	5.3 a			**3.49 E3**	24	**5.02 E3**	22
Zr95	64 d	**5.49 E4**	27	**2.70 E4**	16		
Nb92m	10 d	**3.00 E4**	30				
Nb95	35 d	**3.88 E4**	21	**3.74 E4**	9		

Table 4-4 Alloy A, calculation related results

Product	f_D* EASY	ψ	*C/E*	± Exp.	± EASY	Generic pathways EASY		σ Exp.	Remarks	
	%			%	%		%	mb		
Sc46	98	1.00	**0.95**	**15**	23	Ti46(n,p) Ti47(n,d)	90 10	104.	g+m g+m	
Sc47		1.00	**0.50**	**15**	11	Ti47(n,p) Ti48(n,d) V51(n,nα) V50(n,α)	46 24 26 4			
Cr51	0.03	1.00	**0.78**	**25**	0.5	V51**(p,n)** Fe54(n,α) Cr52(n,2n)	86 7 <7		EASY uncertainty realistic ?	
Mn54	0.4	1.00	(0.83)	15	5	Fe54(n,p) V51**(α,n)** Mn55(n,2n)	97 1 <1		Fe content of sample ??	
Co57	0.8 E-2	1.00	(0.21)	15	28	Ni58(n,d) Ni58(n,2n)Ni57(β^+)	97 3			Ni content of sample ??
Co58	1.3	1.00	(0.34)	15	22	Ni58(n,p)	100		g+m	
Co60	0.02	1.00	(0.22)	28	27	Ni60(n,p Ni61(n,d)	97 3		g+m g+m	
Zr95	0.1	1.00	**0.66**	**25**	23	Zr96(n,2n) Mo97(n,h) Zr94***(n,γ)*** Mo98(n,α)	75 <19 5 1			

Table 4-4 continued

Product	f_D^* EASY	ψ	*C/E*	± Exp.	± EASY	**Generic pathways** EASY		σ Exp.	**Remarks**	
	%			%	%		%	mb		
Nb95	0.2	1.00	(<0.68)	17	25	Mo95(n,p)	<48		g+m	
						Zr96(n,2n)Zr95(β^-)	23		g+m	Pathway shares
						Mo96(n,d)	20			given for
						Mo97(n,h)Zr95(β^-)	6			T_c = 41.0 d
						Zr94***(n,γ)***Zr95(β^-)	2			
						Mo97(n,t)	1			
Nb92m	0.07	1.00	(<0.48)	40	24	Nb93(n,2n)	<76			
						Mo92(n,p)	24			

Table 4-5 Alloy B, calculation related results

Product	f_D^* EASY	ψ	*C/E*	± Exp.	± EASY	**Generic pathways** EASY		σ Exp.	**Remarks**	
	%			%	%		%	mb		
Sc46	98	1.00	**0.99**	**15**	23	Ti46(n,p) Ti47(n,d)	90 10	100.	g+m g+m	
Cr51	0.7	1.00	**1.05**	**15**	5	Cr52(n,2n) V51**(p,n)**	99 1	45.6		
Mn54	0.4	1.00	(1.83)	15	5	Fe54(n,p) Mn55(n,2n) V51**(α,n)**	94 5 1		Fe content of sample ??	
Co57	0.004	1.00	(0.14)	15	28	Ni58(n,d) Ni58(n,2n)Ni57(β+)	97 3			Ni content of sample ??
Co58	0.6	1.00	(0.20)	15	22	Ni58(n,p)	100		g+m	
Co60	0.009	1.00	(0.12)	27	27	Ni60(n,p) Ni61(n,d)	97 3		g+m g+m	

4.3 Nickel and copper

4.3.1 Description of experiment

As a complement to the work on steels and other engineering alloys, pure nickel was investigated to check the production of Co radioisotopes, in particular, Co-60 with its long half life and high specific contribution to the γ dose rate. Pure copper was included in the experiment because it enables another important pathway for Co-60 production.

Table 4-6 Activation parameters

	Ni sample	Cu sample
T_A	7331 s	
Φ	1.010 E11 $cm^{-2}s^{-1}$	9.146 E10 $cm^{-2}s^{-1}$
m	0.952 g	0.917 g
Sample shape	square 10mm × 10mm	
Sample thickness	1.0 mm	1.0 mm

The nickel material, specified by the supplier as 99% pure, was not analyzed for impurities, as only the products from Ni were interesting. The copper material, specified by the supplier as 99.997% pure, was analyzed by Adelhelm et al. at the Materials Research Institute of this Centre for Fe, Co and Ni, after the activation product Fe-59 surprisingly had been identified (see below). None of those impurities was found. The minimum detectable concentrations are quoted in Table 4-7.

Table 4-7 Elemental composition

Element	Ni sample	Cu sample
	weight %	weight %
Fe		<0.0001
Co		<0.0003
Ni	99	<0.0003
Cu		99.997

For this experiment, the neutron fluence was obtained by comparing the Ni-57 reaction rate of the upstream monitor foil with the corresponding one found in the spectrum measurement.

4.3.2 Results and discussion

The results are given in Tables 4-8 to 4-11.

Table 4-8 Nickel, experimental results

Product	≈ $T_{½}$	T_c = 8880 s ≈ 2.5 h		T_c = 89340 s ≈ 25 h		T_c = 718910 s ≈ 8 d		T_c = 3024300 s ≈ 35 d	
		A_{sp}	±	A_{sp}	±	A_{sp}	±	A_{sp}	±
		Bq/kg	%	Bq/kg	%	Bq/kg	%	Bq/kg	%
Fe59	45 d			**2.35 E5**	24	**2.10 E5**	5	**1.37 E5**	3
Co56	77 d					**2.36 E4**	19	**9.89 E3**	35
Co57	272 d	**1.58 E7**	2	**1.67 E7**	0.6	**1.71 E7**	0.4	**1.60 E7**	0.1
Co58	71 d	**1.77 E8**	1	**2.41 E8**	0.4	**2.37 E8**	0.2	**1.85 E8**	0.4
Co60	5.3 a			**4.79 E5**	13	**4.63 E5**	2	**4.73 E5**[a]	1
Co61	1.7 h	**7.11 E7**	13						
Ni57	36 h	**1.42 E8**	1.4	**9.20 E7**	2	**3.08 E6**	5		
Ni65	2.5 h	**5.49 E6**	15						

[a] Co-60 measured by direct comparison with calibrated Co-60 sample

Table 4-9 Nickel, calculation related results

Product	f_D* EASY	ψ	*C/E*	± Exp.	± EASY	**Generic pathways** EASY		σ Exp.	**Remarks**
	%			%	%		%	mb	
Fe59	0.1	1.00	**0.95**	**10**	11	Ni62(n,α) Ni60(n,2p)	98 2	4.60	
Co56		1.00	**2.56**	**25**	10	Ni58(n,t)	100	4.4 E-2	
Co57	0.8	1.00	**0.81**	**10**	29	Ni58(n,d)	100	107.	
Co58	99	1.00	**0.79**	**10**	29	Ni58(n,p)	100	437.	g+m
Co60	0.1	1.00	**0.84**[a]	**10**	26	Ni60(n,p) Ni61(n,d)	98 2	55.2	g+m
Co61	0.9	1.02	**1.47**	**15**	19	Ni61(n,p) Ni62(n,d) Ni64(n,α)Fe61(β^-)	76 21 3		
Ni57	30	1.00	**0.96**	**10**	5	Ni58(n,2n)	100	5.42	
Ni65	0.3	1.01	(0.96)	20	115	Ni64***(n,γ)***	100		Low en. flux uncertain

[a] Co-60 measured by direct comparison with calibrated Co-60 sample

Table 4-10 Copper, experimental results

Prod.	$\approx T_{½}$	T_c = 10680 s ≈ 3 h		T_c = 82260 s ≈ 23 h		T_c = 695340 s ≈ 8 d		T_c = 2929380 s ≈ 34 d		T_c = 7347360 s ≈ 85 d	
		A_{sp}	±	A_{sp}	±	A_{sp}	±	A_{sp}	±	A_{sp}	±
		Bq/kg	%	Bq/kg	%	Bq/kg	%	Bq/kg	%	Bq/kg	%
Fe59	45 d					**8.55 E3**	29	**5.41 E3**	18	**3.03 E3**	20
Co58	71 d					**1.65 E3**	50				
Co60	5.3 a			**2.56 E5**	6.5	**2.68 E5**	2	**2.71 E5**	0.8	**2.66 E5**	1
Co61	1.7 h	**3.74 E7**	20								
Ni65	2.5 h	**3.92 E8**	2.4	**1.67 E6**	6.5						
Cu64	13 h	**4.09 E9**	8	**1.40 E9**	1.6						

Table 4-11 Copper, calculation related results

Product	f_D* EASY	ψ	C/E	± Exp.	± EASY	Generic pathways EASY		σ Exp.	Remarks
	%			%	%		%	mb	
Fe59	1.2[a]	1.00	**0.006**	**20**		Co59(n,p)	100		Cu63(n,pα): see text
Co58		1.00	**0.17**	**50**		Co59(n,2n)	100		Cu63(n,2nα):see text
Co60	99.9	1.00	**0.91**[b]	**10**	22	Cu63(n,α)	100	15.0	g+m
Co61	0.2	1.02	**1.31**	**20**	200	Cu65(n,nα)	100	0.71	
Ni65	28	1.01	**0.89**	**10**	30	Cu65(n,p)	100	7.4	
Cu64	72	1.00	**0.77**	**10**	6	Cu65(n,2n) Cu63(n,γ)	90 10	157.	

[a] from experiment
[b] Co-60 measured by direct comparison with calibrated Co-60 sample

For the nickel sample, no gross discrepancies are observed except the overestimated ^{58}Ni(n,t)^{56}Co reaction.

In the copper sample, Fe-59 was surprisingly detected. In the EASY calculation, a 3 ppm Co impurity was assumed (cf. Table 4-7) to check if the ^{59}Co(n,p)^{59}Fe reaction could explain this. The *C/E* demonstrates that the Fe-59 cannot be explained in this way. Likewise, a 3 ppm Ni impurity would not suffice, as seen by comparison with the Fe-59 activity found in the nickel sample. Neither could a 1 ppm Fe impurity, providing the path ^{58}Fe(n,γ)^{59}Fe, suffice in view of the low epithermal and thermal flux fraction of the neutron spectrum and the Fe-58 isotopic concentration of only 0.28%. Therefore, the Fe-59 must be the product of the ^{63}Cu(n,pα) or/and the ^{65}Cu(n,tα) reaction. These rather exotic reaction types are not included in EAF-99. The reaction thresholds of ^{63}Cu(n,pα)^{59}Fe and ^{65}Cu(n,tα)^{59}Fe as calculated from the masses[Au95] are 6.7 MeV and 16.2 MeV respectively. Since the emitted particles require several MeV of kinetic energy to overcome the Coulomb barrier, the effective threshold in either case is correspondingly higher, and only the very small tail of our neutron spectrum extending beyond 20 MeV could induce the latter reaction. For emission of any possible particle combination x other than pα in ^{63}Cu(n,x)^{59}Fe, such as 2pt, d ^{3}He, p 2d etc., the thresholds are beyond 25 MeV. Similarly, alternative channels in ^{65}Cu(n,x)^{59}Fe are ruled out. Two-step reactions, such as ^{63}Cu(n,α)^{60}Co(n,d)^{59}Fe, ^{63}Cu(n,p)^{63}Ni(n,nα)^{59}Fe, ^{63}Cu(n,d)^{62}Ni(n,α)^{59}Fe etc., are excluded because the effective ^{59}Fe production cross section would then be the product of two small cross sections. Given, e.g., the ^{63}Cu(n,α)^{60}Co reaction rate as observed in this experiment, a ^{60}Co(n,d)^{59}Fe cross section of several megabarns would be required to explain the observed ^{59}Fe activity by the first of the above processes. Therefore, the observed reaction can be identified as ^{63}Cu(n,pα)^{59}Fe, even though only the product nuclide and no emitted particles were detected. The cross section averaged over the part of our spectrum above the 6.7 MeV threshold, calculated as

$$\sigma = F\, N_{59} / (N_n\, N_{63}) \tag{9}$$

from the area F of the sample and the numbers N_n of neutrons above threshold, target nuclei N_{63} and product nuclei N_{59}, is 30 μb ±20%.

The assumed 3 ppm Co content also appears insufficient to explain the Co-58 activity. However, a new calculation by Forrest [Fo02] has shown that an additional 3 ppm Ni impurity (which was not assumed in our own calculation) leads to a reasonable *C/E*, due to the ^{58}Ni(n,p)^{58}Co reaction.

The remaining products found in the copper sample do not show any gross discrepancies.

4.4 Lithium orthosilicate

4.4.1 Description of experiment

The tritium breeder material lithium orthosilicate Li_4SiO_4 is a granulate consisting of glasslike pebbles. This is not practical as an activation sample for our experiments, in which a well defined sample geometry is required. Therefore, solid discs were produced from the granulate by a hot pressing/sintering process at a specialized laboratory (HITEC Materials, Karlsruhe). The pressing tool consisted of graphite. To remove surface layers that might have a modified composition, the sintered discs were ground to the final dimensions of 10 mm diameter and 1.5 mm thickness using diamond grinding tools. One of the discs was activated according to Table 4-12.

Table 4-12 Activation parameters for Li_4SiO_4

T_A	168600 s = 46.833 h
Φ	1.230 E11 $cm^{-2}s^{-1}$
m	0.2828 g
Sample shape	circular, 10mm diameter
Sample thickness	1.5 mm

The temperature during irradiation apparently went high enough to cause some softening of the glassy lithium orthosilicate. As a result, the upstream graphite foil (see Sect. 2.3) was stuck or soldered to the sample so that it could not be removed. The graphite contains some implanted Co-56 generated in the nickel monitor foil. This prevented us from a quantitative determination of Mn-56, the product of the $^{56}Fe(n,p)$ reaction, because the main γ line of Mn-56 at 847 keV is also emitted by Co-56.

The original granulate, produced by Schott Mainz, batch no. 98/2-3, had been analyzed by Adelhelm et al. at Karlsruhe (Table 4-13). The mass of the sintered discs was not sufficient for a new detailed analysis. As will be seen, the activation results indicate that the titanium impurity concentration seems to have been reduced by the pressing/sintering process.

For fluence determination in this experiment, the upstream monitor foil was directly compared to the upstream monitor foil of the Ni-Cu activation.

4.4.2 Results and Discussion

The results are given in Tables 4-14 and 4-15.

For the very short lived Al isotopes produced, the experimental uncertainty given for *C/E* includes contributions accounting for the limited time resolution of target current registration and the uncertainty of the shortest cooling time.

With regard to activation products from the main constituents Li and Si we note the following:

Table 4-13 Elemental composition of Li_4SiO_4 granulate

Element	weight %	± weight %
Li	22.12	0.13
Si	23.30	0.03
O	54.29	
C	0.108	0.0005
Na	0.0033	0.0010
Mg	0.0029	0.0006
Al	0.115	0.023
K	0.0076	0.0005
Ca	0.0059	0.0001
Ti	0.0214	0.0004
Cr	< 0.0006	
Mn	0.00030	0.00004
Fe	0.0143	0.0001
Co	< 0.0004	
Ni	< 0.0006	
Cu	< 0.0004	
Zn	< 0.0002	
Zr	0.0046	0.0002

Be-7 is a relatively important case of a sequential charged-particle reaction product. It is slightly underestimated by EASY-99. In the present material, it contributes up to a few percent of the γ dose rate. In a material of higher purity, its relative importance would increase; in absolutely pure Li_4SiO_4 it would be the only product with $T_{1/2}$ >21 h and would consequently be dominating at longer cooling time. Improving the calculation of this specific activation process may be worthwhile, as it will occur, together with its very weak analogue $^6Li(d,n)^7Be$, in any lithium based tritium breeder material in DT fusion reactors. (The $^6Li(d,n)^7Be$ reaction will even occur in an isotopically pure Li-6 breeder material).

Mg-27, Al-28, Al-29 are the essential products from Si. They are all slightly overestimated. In a 14-MeV neutron activation experiment compared with EASY-99, Seidel et al.[Se00] found *C/E* closer to unity, especially for the two Al isotopes.

Mg-28, produced from Si-29 by the exotic, weak (n,2p) reaction, is predicted within the very large calculational uncertainty. This is the only case observed in our experiments where an (n,2p) reaction constitutes the principal production pathway.

Table 4-14 Li_4SiO_4, experimental results

Product	≈ $T_{½}$	T_c = (900±60) s = 15 min		T_c = (1140±60) s = 19 min		T_c = 6960 s ≈ 2 h		T_c = 29820 s ≈ 8 h	
		A_{sp}	±	A_{sp}	±	A_{sp}	±	A_{sp}	±
		Bq/kg	%	Bq/kg	%	Bq/kg	%	Bq/kg	%
Be-7	53d							**3.62 E5**	50
Mg-27	9 min	**1.11 E8**	7	**8.77 E7**	4				
Mg-28	21 h					**2.50 E5**	35	**1.10 E5**	25
Al-28	2 min	**4.44 E8**	3	**1.41 E8**	4				
Al-29	7 min	**1.99 E8**	3	**1.41 E8**	2				
Na-22	2.6 a								
Na-24	15 h	**9.48 E7**	5	**9.81 E7**	2	**8.98 E7**	1	**6.87 E7**	0.4
Ca-47	4.5 d								
Sc-46	84 d								
Sc-47	3.4 d					**3.68 E5**	20		
Sc-48	44 h					**5.50 E5**	30		
Cr-51	28 d								
Mn-54	312 d								
Mn-56	2.6 h								
Y-88	107 d								
Zr-89	78 h								

Table 4-14 continued

Product	≈ $T_{½}$	T_c = 109620 s ≈ 30 h		T_c = 375660 s ≈ 4 d		T_c = 1841820 s ≈ 21 d		T_c = 9684540 s ≈ 112 d	
		A_{sp}	±	A_{sp}	±	A_{sp}	±	A_{sp}	±
		Bq/kg	%	Bq/kg	%	Bq/kg	%	Bq/kg	%
Be-7	53d	**3.55 E5**	13	**3.70 E5**	5	**3.06 E5**	2	**9.60 E4**	7
Mg-27	9 min								
Mg-28	21 h	**7.01 E4**	13						
Al-28	2 min								
Al-29	7 min								
Na-22	2.6 a							**6.38 E2**	60
Na-24	15 h	**2.45 E7**	0.4	**7.92 E5**	2				
Ca-47	4.5 d			**2.59 E3**	80	**6.32 E2**	65		
Sc-46	84 d	**2.11 E4**	40	**1.72 E4**	10	**1.52 E4**	4	**7.92 E3**	7
Sc-47	3.4 d	**2.65 E5**	3	**1.46 E5**	2	**6.68 E3**	10		
Sc-48	44 h	**3.98 E5**	5	**1.18 E5**	3				
Cr-51	28 d					**9.06 E3**	25		
Mn-54	312 d	**1.98 E4**	40	**1.06 E4**	12	**1.50 E4**	4	**1.28 E4**	6
Y-88	107 d					**2.22 E3**	20	**1.34 E3**	25
Zr-89	78 h	**6.07 E4**	18	**3.55 E4**	10				

Table 4-15 Li_4SiO_4, calculation-related results

Product	f_D^* EASY	ψ	*C/E*	± Exp.	± EASY	**Generic pathways** EASY		σ Exp.	**Remarks**
	%			%	%		%	mb	
Be-7	4.8	1.00	**0.68**	**10**	--	Li7**(p,n)**	100		Li6**(d,n)** contribution??
Mg-27	8.4	1.14	**1.49**	**10**	9	Si30(n,α) Al27(n,p) Si28(n,2p)	71 27 2		
Mg-28	0.07	0.99	**0.39**	**12**	199	Si29(n,2p) Si30(n,h)	99 1	8.6 E-3	
Al-28	53	1.27	**1.62**	**25**	25	Si28(n,p)	100	63.	
Al-29	26	1.18	**1.59**	**15**	25	Si29(n,p) Si30(n,d)	98 2	32.	
Na-22	2.5	1.00	**1.36**	**60**	24	Na23(n,2n)	100	4.6	
Na-24	97	0.98	**0.83**	**20**	22	Al27(n,α) Mg24(n,p)	96 4	34.	g+m
Ca-47	3	1.00	(6.9)	70	89	Ca48(n,d)K47(β-) Ca48(n,2n) Ti50(n,α)	89 5 6		

Table 4-15 continued

Product	f_D* EASY	ψ	*C/E*	± Exp.	± EASY	**Generic pathways** EASY		σ Exp.	**Remarks**
	%			%	%		%	mb	
Sc-46	56	1.00	(2.79)	10	23	Ti46(n,p)	90		
						Ti47(n,d)	10		
Sc-47	0.6	1.00	(2.69)	10	12	Ti47(n,p)	64		
						Ti48(n,d)	33		Ti content of
						Ti49(n,t)	1		disc sample ?
						Ca48(n,d)K47(β-)Ca47(β-)	2		
Sc-48	22	0.99	(2.66)	10	5	Ti48(n,p)	99		
						Ti49(n,d)	1		
Cr-51	0.2	1.00	(<1.82)	25	36	Cr52(n,2n)	<58		Cr in sample
						Fe54(n,α)	42		« <6 ppm »
Mn-54	13	1.00	**0.98**	**10**	4	Fe54(n,p)	87		
						Mn55(n,2n)	13		
Y-88	0.01	1.00	(1.8E-3)	20	60	Zr90(n,t)	100		Y impurity ?
Zr-89	1.0	1.00	(6.93)	**10**	25	Zr90(n,2n)	100	13.7	

Concerning activation products from the impurities we note:

Na-24 originates from an Al impurity of only 0.1 weight%. Nevertheless it contributes up to 97% to the γ dose rate. It is calculated within uncertainty. Minimizing the Al impurity in the material may be worthwhile.

Ca-47: The *C/E* indicates either a problem of the ^{48}Ca(n,d) cross section in EAF or a reduced Ca impurity in the sample.

Sc-46, 47, 48, all from the Ti impurity, are all overestimated 2.7 times. This clearly points to an incorrect Ti concentration in the sample. It is not clear if the hot pressing/sintering process may have altered this concentration. The vanadium-titanium alloys experiment (Sect. 4.2) gave a much better *C/E* for Sc-46.

Cr-51: The Cr content of the sample may be close to zero (see Table 4-13), leaving only the ^{54}Fe(n,α) pathway. This would result in $C/E \approx 0.76$, compatible within uncertainty with unity.

Y-88 is underestimated 500-fold. This suggests an yttrium impurity in the sample, which would permit the ^{89}Y(n,2n)^{88}Y pathway.

Zr-89: like for Ca-47, the *C/E* indicates either a cross section problem or a reduced Zr impurity in the sample.

In addition to the products reported here, small activities of heavier radionuclides (Nb-92m, Ag-106, Ir-190 and -192, Au-195) were detected. These must be due to trace impurities of corresponding masses, that were not searched for in the chemical analysis.

4.5 Eurofer-97

4.5.1 Description of experiment

The reduced-activation steel Eurofer-97 contains about 1% tungsten. This heavy element consists of five stable isotopes, which can produce a considerable number of (mostly short lived) gamma emitting radionuclides. Tungsten is also considered for use in fusion technology as a pure material or alloy base material. In our experiment, therefore, it appeared useful to activate a Eurofer-97 sample and a pure tungsten sample simultaneously. Table 4-16 gives the activation parameters for these two samples. All further data and results for the tungsten sample, however, are given in section 4.6.

Table 4-16 Activation parameters

	Eurofer-97	Tungsten, sample W2
T_A	155100 s = 43.08 h	
Φ	1.22 E11 $cm^{-2}s^{-1}$	1.48 E11 $cm^{-2}s^{-1}$
m	1.1838 g	1.7819 g
Sample shape	square 10mm × 10mm	
Sample thickness	1.5 mm	1.0 mm

The composition of Eurofer-97 as analyzed by Adelhelm et al. at Karlsruhe is given in Table 4-17. The material for this analysis was taken adjacent to the activation sample from the same plate, so as to minimize any effects of inhomogeneous distributions of constituents or impurities.

Table 4-17 Elemental composition of Eurofer-97

Element	weight %	± weight %
C	0.104	0.005
Al	0.0051	0.0001
Si	0.043	0.0005
P	<0.04	
S	0.004	0.001
Ti	0.004	
V	0.204	0.004
Cr	9.21	0.12
Mn	0.502	0.012
Fe	balance	
Co	0.0067	0.00005
Ni	0.0214	0.002
Cu	0.0049	0.00005
Nb	0.0012	0.0003
Mo	<0.0008	
Ta	0.145	
W	1.148	0.028

During the activation a beam overcurrent accident led to some melting damage on the Be target. The samples and monitor foils were not noticeably damaged, but the shape and location of the neutron generating volume within the target block were different during the second part of the 2-day irradiation from what they were during the first part. This may possibly have modified the relationship between flux on the monitor foil and flux on the samples, which would explain why even the Ni moni-

tor foil comparison with the Ni-Cu activation, applied so successfully for normalizing the LS activation fluence, did not lead to a credible result in this case. A normalization factor was then derived for this experiment by comparing the ^{58}Ni(n,d)^{57}Co reaction rates in the Eurofer sample and the Ni sample of the Ni-Cu experiment. This is, in principle, a 'cleaner' method than the one relying on monitor foils, as it is insensitive to any geometry differences between sample and monitor foil. However, the Ni content of the Eurofer sample is only known to within ±10%, which leads to an additional uncertainty component in the results. We therefore use, for all results from the Eurofer and W2 samples, ±15% instead of the usual ±10% estimated (covariant) uncertainty stemming from the spectrum together with the fluence normalization.

Also due to the beam accident, the time history of the neutron flux density on the sample cannot be reconstructed from the registered current data. Such reconstruction and subsequent calculation of ψ factors (see Sect. 3.2) would be required for calculating specific activities of short lived products. Therefore, results from these two samples are given only for products with $T_{1/2} \geq 3.4$d. Measuring the short lived products in Eurofer with our method would suffer in any case from the very strong ^{56}Fe(n,p)^{56}Mn(2.6h) reaction, as the Compton background from the Mn-56 γ lines would cover up most of the other lines. For tungsten, a separate activation for determining the short lived products was performed (see below).

4.5.2 Results and discussion

The Eurofer results are shown in Tables 4-18 and 4-19. Considering specific product nuclides we note the following:

Sc-46, 47: The real Ti content of the sample might be higher than 40 ppm (note that the chemical analysis, Table 4-17, does not give an uncertainty for Ti). This would explain the low *C/E* ratios. In the experiment on V-Ti alloys (see section 4.2), the *C/E* for Sc-46 were near unity.

Mn-52: The ^{54}Fe (n,t) cross section, which has its threshold at 12.7 MeV neutron energy, appears to be strongly overestimated in EAF-99.

Co-56: According to EASY, purely due to a sequential proton induced reaction. Production by the ^{58}Ni (n,t) reaction is very small because of the low Ni content of the sample.

Co-57: Result used for fluence normalization of the experiment (see above).

W-181: This nuclide emits only two γ lines, either of which coincides with a line of another nuclide within experimental energy resolution. The *C/E* given here was obtained from the 136 keV γ peak area after subtracting a fraction corresponding to the Co-57 line at this energy. Note the large experimental (statistical) uncertainty resulting from this procedure.

Table 4-18 Eurofer, experimental results

Product	≈ $T_{½}$	T_c = 178440 s ≈ 50 h		T_c = 1036560 s ≈ 12 d		T_c = 3552540 s ≈ 41 d		T_c = 16338840 s ≈ 189 d	
		A_{sp}	±	A_{sp}	±	A_{sp}	±	A_{sp}	±
		Bq/kg	%	Bq/kg	%	Bq/kg	%	Bq/kg	%
Sc46	84d			**1.42 E4**	10			**2.99 E3**	11
Sc47	3.4d	**3.70 E5**	6	**4.47 E4**	13				
V48	16d					**1.95 E4**	14		
Cr51	28d			**2.60 E8**	0.1	**1.21 E8**	0.1	**3.28 E6**	1
Mn52	5.6d	**1.23 E5**	45	**2.85 E4**	15	**1.10 E3**	30		
Mn54	312d			**8.26 E7**	0.1	**7.72 E7**	0.1	**5.79 E7**	0.1
Fe59	45d			**1.81 E5**	3	**1.20 E5**	2	**1.31 E4**	4
Co56	77d			**2.95 E4**	4	**2.36 E4**	3	**5.45 E3**	4
Co57	272d			**8.09 E4**	5	**7.79 E4**	3	**5.99 E4**	4
Co58	71d			**1.12 E6**	0.6	**8.47 E5**	0.6	**2.10 E5**	1
Co60	5.3a			**4.66 E3**	15	**3.77 E3**	11	**3.22 E3**	6
Nb92m	10d			**7.26 E4**	3	**6.73 E3**	14		
Hf181	42d			**1.15 E4**	30				
Ta182	114d			**1.12 E6**	0.7	**9.36 E5**	0.7	**4.01 E5**	2.6
Ta183	5d	**2.10 E5**	24	**4.25 E4**	22				
W181	121d			**7.90 E6**	30				
W185	75d					**9.16 E6**	67	**1.30 E6**	50

Table 4-19 Eurofer, calculation-related results

Product	f_D* EASY	*C/E*	± Exp.	± EASY	**Generic pathways** EASY		σ Exp.	**Remarks**	
	%		%	%		%	mb		
Sc46	0.02	(0.60)	15	23	Ti46(n,p) Ti47(n,d)	90 10	165.	g+m	Ti content of sample = 40 ppm ± ??
Sc47	?	(0.47)	15	12	Ti47(n,p) Ti48(n,d) V50(n,α) V51(n,nα)	38 20 6 36			
V48	0.5	**1.58**	**20**	60	Cr50(n,t)	100	0.27		
Cr51	6	**0.89**	**15**	4	Cr52(n,2n) Fe54(n,α)	77 23			
Mn52	7	**49.**	**20**	57	Cr52**(p,n)** Fe54(n,t)	2 98	 0.090	 g+m	
Mn54	99	**0.95**	**15**	5	Mn55(n,2n) Fe54(n,p)	4 96	 287		
Fe59	0.3	(0.80)	15	31	Fe58***(n,γ)*** Co59(n,p) Ni62(n,α)	79 20 1		Low energy flux uncertain	
Co56	0.5	**3.6**	**15**	---	Fe56**(p,n)**	100		Ni58(n,t) ??	
Co57	0.004	*0.90*	15	28	Fe57**(p,n)** Ni58(n,d)	2 96		*used for fluence normalization*	

Table 4-19 continued

Product	f_D* EASY	*C/E*	± Exp.	± EASY	Generic pathways EASY		σ Exp.	Remarks
	%		%	%		%	mb	
Co58	1.3	**1.00**	15	20	Co59(n,2n)	11		
					Ni58(n,p)	89		
Co60	0.02	**0.74**	15	22	Co59***(n,γ)***	9		g+m
					Ni60(n,p)	80		
					Ni61(n,d)	2		
					Cu63(n,α)	9		
Nb92m	0.08	**0.58**	15	29	Nb93(n,2n)	95	276.	
					Mo92(n,p)	5		
Hf181		**1.84**	30	16	Ta181(n,p)	57		
					W184(n,α)	43		
Ta182	0.5	(0.30)	15	90	Ta181***(n,γ)***	94		Low energy flux uncertain
					W182(n,p)	4		
					W183(n,d)Ta182m(IT)	1		
Ta183	0.03	**1.26**	16	44	W183(n,p)	44		Pathway shares
					W184(n,d)	40		refer to T_c = 50 h
					W186(n,α)Hf183(β^-)	16		
W181	0.03	**0.68**	30	26	W182(n,2n)	93	578.	
					W183(n,3n)	7		
W185	0.3 E-4	**0.95**	40	35	W184***(n,γ)***	4		
					W186(n,2n)	96	434.	g+m

4.6 Tungsten

4.6.1 Description of experiment

Two samples of 1.0 mm tungsten plate (nominally 99.95% W, supplied by Alfa Aesar, Karlsruhe) were investigated. One of them, denoted W2, was activated together with the Eurofer-97 sample as described in the previous section. Because of the overcurrent accident reported there, reliable results could be derived only for products having sufficiently long half lives. As tungsten produces a considerable number of shorter lived products as well, a second activation on a new sample, W1, was carried out in addition (Table 4-20).

The neutron fluence on the W2 sample was, obviously, the same as on the Eurofer sample except for the geometrical flux decrease measured by Ni monitor foils in the usual way. The W1 activation fluence was normalized to the W2 activation fluence by equating the specific Ta-183 production rates in the two samples.

Table 4-20 Activation parameters for sample W1

T_A	7630 s
Φ	1.16 E11 $cm^{-2}s^{-1}$
m	1.7853 g
Sample shape	10mm × 10mm square
Sample thickness	1.0 mm

The interest was only in the activation products of tungsten, so that a complete elemental analysis of the tungsten samples was not required. However, the material was analyzed by a specialized laboratory (H.C. Starck, Goslar, Germany) for the neighbouring elements Hf, Ta, Re and Os, because these may produce, under fast neutron irradiation, some of the same radionuclides that are expected to originate from tungsten. None of these four impurity elements was found, at a detection limit of 5 ppm for each of them. In order to estimate the possible effects of such impurities, a content of 5 ppm each of Hf, Ta, Re and Os was assumed in the EASY-99 calculations (see Table 4-21).

Table 4-21 Elemental composition of tungsten samples assumed in EASY calculations

Element	Z	weight %
Hf	72	0.0005
Ta	73	0.0005
W	74	99.9980
Re	75	0.0005
Os	76	0.0005

4.6.2 Results and discussion

The results from sample W2 are shown in Tables 4-22 and 4-23 and those from sample W1 in Tables 4-24 and 4-25.

In contrast to the experiments on materials of lower atomic numbers, no products of sequential charged-particle reactions could be identified. This may be due to the high coulomb barrier of tungsten ($Z = 74$), which impedes any reaction involving charged particle absorption or emission.

Likewise, the long-lived product Hf-178n ($T_{1/2} = 31$a) of the W182(n,nα) reaction could not be identified. EASY-99 predicts 4.0E+02 Bq/kg for this nuclide in sample W2, several orders of magnitude less than the minimum detectable activity.

The nuclides in this mass region have many levels, and some emit numerous γ lines. In several cases, product nuclides that might have been detectable judging by their activity and γ line intensities could not be identified and determined because of duplication with lines from other nuclides at the same energy (within the experimental γ energy resolution of about 1.7 keV).

Considering some of the product nuclides in sample W2 we note the following:

Hf-179n: As seen in the 'pathways' column, this is the only experimentally identified product in which a target element other than W, if present at the ppm level, would play a role. The > and < symbols with the pathway percentages reflect the incomplete information about the Hf impurity concentration ('< 5 ppm').

Ta-178: This nuclide has two states with β^+ decay half lives of about 9 min and 2.4 hours. According to some sources[Pf98, Fi96] it is not clear which of these is the ground state. The EASY output lists 'Ta-178' without indicating to which half life it refers. The β^+ decays of the two states can be distinguished experimentally by their different accompanying γ lines. The result in Table 4-23, $C/E = 0.96$, is obtained assuming that the specific activity calculated by EASY refers to the 9 min state. Assuming that it refers to the 2.4 h state would lead to $C/E \approx 400$.

The pathway percentages listed for Ta-178 refer to sample W2 at 1.2 d cooling time. The percentages are time dependent, because the production by the W180(n,t) reaction is prompt, while the production by the W180(n,3n)W178(β^+) chain is greatly delayed by the 22 d half life of the β^+ decay. Since the Ta-178 observed is essentially coming from the latter pathway, its radiation appears with this long effective half life. The z_M correction factor (see Sect. 2.8.2) for Ta-178 was, therefore, taken for this half life and not for 9 minutes.

Ta-182: The great difference between this C/E ratio and the one found for the same product and same EASY version in Eurofer-97, $C/E = 0.29$, is explained by the different production paths.

Table 4-22 Sample W2, experimental results

Product	$\approx T_{½}$	T_c = 99720 s ≈ 1.2 d		T_c = 551160 s ≈ 6 d		T_c = 2788140s ≈ 32 d		T_c = 16414020 s ≈ 190 d	
		A_{sp}	±	A_{sp}	±	A_{sp}	±	A_{sp}	±
		Bq/kg	%	Bq/kg	%	Bq/kg	%	Bq/kg	%
Hf179n	25 d			**2.70 E4**	22	**6.91 E3**	8		
Hf181	42 d			**5.13 E5**	0.6	**3.49 E5**	0.6	**2.71 E4**	3
Ta178	9 min			**4.06 E5**	6	**1.85 E5**	7		
Ta182	114 d	**1.43 E6**	2.4	**1.37 E6**	0.4	**1.19 E6**	0.4	**4.69 E5**	0.3
Ta183	5 d	**2.37 E7**	7	**1.08 E7**	2.7	**3.22 E5**	2		
W181	121 d					**5.87 E8**	0.8	**2.20 E8**	0.4
W185	75 d					**7.41 E8**	0.5	**1.76 E8**	0.8

Table 4-23 Sample W2, calculation-related results

Product	f_D* EASY	ψ	*C/E*	± Exp.	± EASY	**Generic pathways** EASY		σ Exp.	**Remarks**
	%			%	%		%	mb	
Hf179n	0.03		**0.46**	**30**	40	W182(n,α) W183(n,nα) Hf180(n,2n) Hf179(n,n')	>84 >11 <4 <1		
Hf181	5.3		**1.59**	**15**	36	W184(n,α)	98	0.166	
Ta178	0.5		**0.96**	**15**	193	W180(n,3n)W178(β+) W180(n,t)	97 3	17.1	Pathway percentage time dependent, see text
Ta182	86		**1.23**	**15**	32	W182(n,p) W183(n,d)	83 17		
Ta183	5.3		**1.01**	**15**	47	W183(n,p) W184(n,d) W186(n,α)Hf183(β-)	48 43 9		Pathway percentage time dependent, see text
W181	13		**0.74**	**15**	26	W182(n,2n) W183(n,3n)	93 7	531.	
W185	0.04		**0.83**	**15**	35	W186(n,2n) W184***(n,γ)***	96 4	496.	g+m

Ta-183: There is no clear explanation for the *C/E* difference from the Eurofer result, *C/E* = 1.26 ±16%(exp.) ±44%(EASY). Note that the experimental uncertainties contain an estimated 15% uncertainty of the source neutron spectrum and the fluence determination, which is covariant and cannot explain differences between two of our experimental results. However, the absolute quantity of tungsten contained in the Eurofer sample was only 13.6 mg, less than 1% of the pure tungsten sample. The γ line intensities were correspondingly weaker and may have left more room for unnoticed systematic errors, e.g., in identifying close-lying lines. We feel, therefore, that *C/E* = 1.01±15% as found in the pure W sample is the more reliable result.

As one of the three pathways involves a β decay with $T_{1/2}$ = 64 min, the pathway percentages are somewhat time dependent. The quoted percentages refer to sample W1 at zero cooling time.

W-181: Within experimental uncertainty, good agreement with Eurofer result.

W-185: Within experimental uncertainty, good agreement with Eurofer result.

Considering the product nuclides in sample W1 we note:

Hf-180m: For this product the *C/E* deviation from unity is significant even compared with the total uncertainty, i.e., the experimental and EASY uncertainties combined.

W-187: Slight disagreement with Eurofer result. W-187 being an (n,γ) reaction product, these results of our experiments are not recommended for EAF cross section validation. Note the high contribution of W-187 to the total γ dose rate (about 95% at 1 d cooling time), which will be even higher in tungsten irradiated in a fusion reactor neutron spectrum.

Table 4-24 Sample W1, experimental results

Product	≈ $T_{½}$	T_c = 810 s ≈ 14 min		T_c = 1742 s ≈ 29 min		T_c = 10620 s ≈ 3 h		T_c = 52980 s ≈ 15 h		T_c = 269520 s ≈ 3 d		T_c = 1723020 s ≈ 20 d	
		A_{sp}	±	A_{sp}	±	A_{sp}	±	A_{sp}	±	A_{sp}	±	A_{sp}	±
		Bq/kg	%	Bq/kg	%	Bq/kg	%	Bq/kg	%	Bq/kg	%	Bq/kg	%
Hf180m	5.5 h			**2.45 E5**	19	**1.13 E5**	37	**3.15 E4**	42				
Hf182m	61 min			**1.72 E5**	35								
Hf183	64 min	**9.41 E6**	5	**7.61 E6**	1.7	**1.37 E6**	4						
Ta182m	16 min	**2.80 E6**	22	**1.87 E6**	30								
Ta183[a]	5 d			*2.18 E6*	*23*	*2.13 E6*	*16*	*1.85 E6*	*13*	*9.86 E5*	*4*	*9.44 E4*	*1.3*
Ta184	9 h	**1.35 E7**	2.2	**1.26 E7**	0.9	**1.02 E7**	1.6	**4.04 E6**	1.4	**3.42 E4**	7		
Ta185	49 min	**1.97 E7**	7	**5.17 E7**	20	**1.63 E6**	20						
Ta186	10 min	**2.47 E7**	8	**1.20 E7**	34								
W179m	7 min	**1.04 E7**	30										
W187	24 h	**3.67 E8**	4	**3.63 E8**	0.3	**3.35 E8**	1.1	**2.41 E8**	2.5	**4.19 E7**	0.9		

[a] *The Ta-183 result was used to normalize the fluence on this sample (see text).*

Table 4-25 Sample W1, calculation-related results

Product	f_D* EASY	ψ	*C/E*	± Exp.	± EASY	Generic pathways EASY		σ Exp.	Remarks
	%			%	%		%	mb	
Hf180m	0.4	1.00	**3.09**	**20**	51	W183(n,α)	99	0.018	
Hf182m	0.1	1.01	**1.04**	**40**	192	W186(n,nα)	95	0.0020	
						W184(n,h)	5		
Hf183	9	1.01	**1.43**	**15**	54	W186(n,α)	100	0.127	
Ta182m	3E-05	1.02	**2.09**	**25**	57	W183(n,d)	63		
						W182(n,p)	36		
						W184(n,t)	1		
Ta184	28	1.00	**1.21**	**15**	27	W184(n,p)	89		
						W186(n,t)	11		
Ta185	0.7	1.01	**1.04**	**30**	100	W186(n,d)	100	0.338	
Ta186	26	1.02	**1.02**	**15**	42	W186(n,p)	100	0.544	
W179m	0.04	1.02	**1.07**	**30**	37	W180(n,2n)	100	87.	
W187	95	1.00	(0.34)	15	48	W186***(n,γ)***	100		Low energy flux uncertain

Ta-183 is not listed here, because it was used as a basis for fluence normalization.
An independent result for Ta-183 is given in Table 4-23.

5 CONCLUSIONS

The first conclusion from this validation experiment series is that EASY has reached a considerable degree of perfection. The experiments have not revealed any important errors in the FISPACT code, and the EAF cross section file appears to be good enough for many practical purposes such as overall predictions of the radioactivity in specific parts of fusion reactors, the planning of handling facilities, concepts for plant decommissioning, etc. Nevertheless, the experiments described have been useful in a number of cases in improving the cross sections. Large discrepancies with calculational results have been found for some reactions that have thresholds near the neutron energy of 14 MeV, such as, e.g., some (n,t) reactions. The fraction of our neutron spectrum between 14 and 20 MeV is, obviously, testing these cross sections in particular. The SAFEPAQ-II code[Fo01] offers the possibility to include the results of integral experiments in a quantitative fitting procedure to improve the cross section evaluations.

The experimental results obtained under the present task obviously retain their value for future validation of EAF or any other activation cross section files.

In two cases, products of the rare class of reactions emitting two charged particles were observed: $^{29}Si(n,2p)^{28}Mg$ and $^{63}Cu(n,p\alpha)^{59}Fe$. The (n,pα) reactions are not included in EAF up to the 1999 version. Generally, the cross sections of these exotic reactions are small, so that their products usually do not contribute much to the overall activity or gamma dose rate of the irradiated material.

The experiment on lithium silicate has demonstrated, inter alia, the importance of the sequential charged-particle induced $^{7}Li(p,n)^{7}Be$ reaction. This activation reaction will inevitably occur in any reactor blanket breeding tritium from lithium. (Even if the lithium were pure Li-6, a very small amount of Be-7 would still be produced by the analogous sequential reaction $^{6}Li(d,n)^{7}Be$). It may be worthwhile to improve the Cierjacks calculational method for this particular process.

It should be noted that our experimental method in its present form cannot cover all of the necessary cross section validations. Some potential improvements, to be considered in future continuations, are the following:

- The internal-target technique used in the cyclotron work has limited the overall precision both with respect to the neutron spectrum characterization and to the fluence determination (see section 2). This could clearly be improved by using an extracted deuteron beam from a variable-energy cyclotron.

- The accessible range of product half lives is limited. Half lives shorter than a few minutes could be covered by using a fast, automated system to transfer an activated sample to the gamma spectrometer, and sub-second half lives by pulsed activation with in-situ gamma spectroscopy. However, the very short lived products can also be checked in a summary

way by decay heat power measurements. The more important, but more difficult extension of the range may be the one towards long half lives. As long half life means low activity, some improvement would be possible by using a specialized low-level gamma spectrometry facility, but the final limit is the available neutron source intensity.

- Chemical separation prior to the gamma spectrometry or, possibly, mass spectrometric techniques applied to the activated sample could help in many cases, e.g., to measure a rare product in presence of an abundant one that has similar γ ray energies or that spoils the spectrum acquisition by overloading the photon detector. A typical example is the ^{56}Fe(n,p)^{56}Mn reaction in steels. Fe-56 is by far the most abundant nuclide in steels, and the Compton background from the intense γ lines of Mn-56 ($T_{1/2}$ = 2.6h) renders it almost impossible to detect any other, rare γ emitters of comparable half lives in an irradiated steel sample.

  Chemical and mass spectrometric techniques might also help in validating the production cross sections of stable nuclides and those that are radioactive but difficult or impossible to measure by their emitted radiation. An example of the latter class is Fe-55 from the ^{56}Fe(n,2n) reaction. Fe-55 decays by a pure electron capture transition without γ ray emission, the only products being a neutrino, X rays that are not specific to the isotope, and the stable Mn-55 daughter nucleus that cannot be distinguished from the natural manganese impurity present in any iron material. The cross section is quite large. Fe-55 can contribute importantly to the nuclear heating and, with its long half life of 2.73 a, may be important as a target nuclide for further activation reactions. Some effort to validate this particular cross section would appear worthwhile. Further comparable cases are Mn-53 ($T_{1/2}$ = 3.7E6 a), produced by the ^{54}Fe(n,d) reaction, and Ni-63 ($T_{1/2}$ = 100a), produced by the ^{62}Ni(n,γ) and ^{63}Cu(n,p) reactions.

ACKNOWLEDGEMENTS

Most of this work was performed within the Nuclear Fusion Programme of Forschungszentrum Karlsruhe with support from the European Fusion Technology Programme. We thank JAERI Tokai-mura and, in particular, Dr. Y. Ikeda for enabling the joint work under the Fusion Neutronics subtask of the IEA Cooperative Program on Nuclear Technology of Fusion Reactors. We are grateful to Dr. H. Schweickert, Mr. J. Möllenbeck and the cyclotron operating crew for their support in using KIZ, to Dr. C. Adelhelm and her group for several chemical analyses, to Prof. Klaus Seidel for enlightening discussions and to Dr. A. Möslang and Dr. E. Daum for pleasant cooperation in the joint use of the gamma spectrometer.

NOTATION LIST

a	Net mean counting rate in a full energy peak (counts per second of live time)
A	Activity (Bq)
A_{sp}	Specific activity (Bq per kg of sample material)
C/E	Ratio of calculated specific activity over measured specific activity
E_n	Neutron energy
E_γ	Gamma ray energy
f_D^*	Highest contribution of nuclide to sample gamma dose rate at any one of the considered cooling times
h	He-3 nucleus
I_γ	Gamma ray intensity (emitted photons of a specific energy per decaying atom)
k_d	Correction for photon absorption within sample
m	Sample mass
t_B	Time of activation beginning
t_E	Time of activation end
t_M	Time of γ spectrum measurement beginnning
T_A	Duration of activation
T_c	Duration of cooling
T_M	Real duration of γ spectrum measurement
$T_{1/2}$	Half life
z_M	Decay-during-acquisition correction
Z	Atomic number
ε	Absolute detector efficiency (counts in full energy peak per emitted photon)
λ	Decay probability per atom (s^{-1})
$\sigma(E_n)$	Neutron energy dependent cross section per atom
σ	Energy averaged ('one-group') cross section per atom
φ	Differential neutron flux density (n/(s cm^2 unit energy or unit lethargy))
Φ	Integral neutron flux density (n/(s cm^2))
ψ	Correction for time dependence of flux

REFERENCES

Au95
G. Audi and H. Wapstra, Nucl. Phys. A 595 (1995) 409

Br93
J.F. Briesmeister (Ed.), MCNP — A general Monte Carlo n-particle transport code, Version 4A, report LA-12625-M, Los Alamos Nat. Lab., USA, 1993

Ci91
S. Cierjacks et al., Nuclear Data Libraries for the Treatment of Sequential (x,n) Reactions in Fusion Materials Activation Calculation. Report KFK 4867, Kernforschungszentrum Karlsruhe, 1991

Ci93
S. Cierjacks et al., Fusion Technology 24 (1993) 277-287

Fi96
R.B. Firestone et al., Table of Isotopes, 8th edition. Wiley,1996

Fo01
R.A. Forrest, J. Kopecky and J.Ch. Sublet, to be published at
Int. Conf. on Nucl. Data for Science and Technology, Tsukuba, Japan, Oct. 7-12, 2001

Fo02
R.A. Forrest, M. Pillon, U. von Möllendorff and K. Seidel, Validation of EASY-2000 using integral measurements. Report UKAEA FUS 467, United Kingdom Atomic Energy Authority, 2002, www.fusion.org.uk/index.html

Ma99
F. Maekawa, U. von Möllendorff, P.P.H. Wilson and Y. Ikeda,
Fusion Technology 36 (1999) 165-172

Mö93
U. von Möllendorff, unpublished report, Forschungszentrum Karlsruhe, 1993

Mö94
U. von Möllendorff, unpublished report, Forschungszentrum Karlsruhe, 1994

Mö97
U. von Möllendorff, H. Giese and F. Maekawa, unpublished report, Forschungszentrum Karlsruhe, 1997

Mö98
U. von Möllendorff, H. Giese and H. Tsige-Tamirat, in: Fusion Technology 1998 (Eds. B. Beaumont et al.), CEA Cadarache (1998), vol 2 pp. 1449-1452

Pf98
G. Pfennig, H- Klewe-Nebenius and W. Seelmann-Eggebert, Karlsruher Nuklidkarte, 6th ed., improved reprint 1998, Forschungszentrum Karlsruhe

Se00
K. Seidel, Progress Report Nov. 1999 to May 2000, EFF-DOC-725, unpublished

Su98
J.-Ch. Sublet, J. Kopecky and R.A. Forrest, report UKAEA FUS 408, United Kingdom Atomic Energy Authority (1998)

Wi97
P.P.H. Wilson and U. Fischer, in: Fusion Technology 1996 (Eds. C. Varandas and F. Serra), Elsevier (1997), vol. 2, pp. 1575-1578

fusion power

energy for the future

introduction

A simple guide to what Fusion Power is all about, why we need it, and how we hope to achieve it.

research

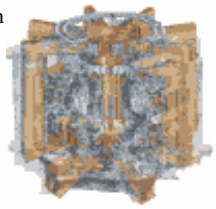

Highlights from the research at Culham, in particular the experimental devices:
JET The world's largest tokamak, operated by UKAEA on behalf of Europe.
MAST The new Spherical Tokamak.
COMPASS-D A highly-adaptable medium-sized tokamak.

technical docs

Some on-line technical papers on UKAEA Fusion research topics, with **new** search facility.

glossary

Explaining the technical terms used in fusion energy research.

ask a question

Have a question about fusion power? Send it to us and we will try to answer. See our replies to frequent questions.

industry

Spin-offs from the fusion research programme are offering real benefits in many industries. Read how we can help boost the achievements of your technology business.

features

Some special topics covered in more depth, including:

- A giant leap for fusion
- The Spherical Tokamak
- START
- Sustainable Development

events

A listing of forthcoming fusion conferences and meetings.

links

Links to Web sites of many fusion research establishments around the world.

opportunities

Career opportunities in fusion research for scientists and engineers.

Direct links to selected topics

What's New | Search

© 1996-2001, United Kingdom Atomic Energy Authority. All rights reserved.

Last update 18 January, 2002 .